

Review

The Effect of High-Temperature Water Vapour on Degradation and Failure of Hot Section Components of Gas Turbine Engines

Kuiying Chen ^{1,*}, Dongyi Seo ¹ and Pervez Canteenwalla ²

¹ Structures and Materials Performance Laboratory, Aerospace Research Centre, National Research Council Canada, Ottawa, ON K1A 0R6, Canada; Dongyi.Seo@nrc-cnrc.gc.ca

² Gas Turbine Laboratory, Aerospace Research Centre, National Research Council Canada, Ottawa, ON K1A 0R6, Canada; Pervez.Canteenwalla@nrc-cnrc.gc.ca

* Correspondence: kuiying.chen@nrc-cnrc.gc.ca

Abstract: For the past decade, the aviation industry has been adopting sustainable aviation fuels (SAF) for use in aircraft to reduce the impact of aviation on climate change. Also, some nations look to SAF as an option for energy security for their military fleets. Understanding the critical impact of alternative fuel sources on hardware will provide the gas turbine industry with strategic options in sustainability and maintainability of the existing and new fleets. The alternative fuels with high hydrogen/carbon ratio (H/C) (such as synthetic paraffinic kerosenes (SPK)) could produce more water vapour content than the conventional jet fuels upon combustion, and this increased water vapour level could exert a significant impact over the long-term durability on hot section components such as the substrate blades, oxidation resistant coatings, thermal barrier coatings (TBCs), environmental barrier coatings (EBCs), resulting in an accelerated degradation of the turbine components. The possible detrimental effect of high-temperature water vapour on degradation and lifespan of hot section components was examined. Examples were specifically given on degradation and spallation of thermally grown oxides (TGO), formation of non-protective oxides and ceramics topcoats in TBCs. Results show that water vapour can lead to volatilization of TGO (Al_2O_3), and is responsible for the formation of non-protective oxides in both Pt-modified β -NiAl and MCrAlY coatings, leading to their early spallation. However, water vapour does not appear to directly affect the ceramic topcoat of the TBC. For EBCs coated on SiC-based substrates, the substrate recession via silica (TGO) volatilization was reviewed. These EBCs were observed undergoing degradation in highly hostile environments, e.g., constantly operating under high temperatures, pressures, and velocities condition in the presence of water vapour steam. The review intends to provide a perspective of high-temperature water vapour effect on the EBCs' topcoat properties such as durability, degradation, crack nucleation and crack growth, and possible guidance for mitigating these degradation effects.

Keywords: thermal barrier coatings; environment barrier coatings; water vapour corrosion; oxidation; thermally grown oxide; topcoat



Citation: Chen, K.; Seo, D.; Canteenwalla, P. The Effect of High-Temperature Water Vapour on Degradation and Failure of Hot Section Components of Gas Turbine Engines. *Coatings* **2021**, *11*, 1061. <https://doi.org/10.3390/coatings11091061>

Received: 7 July 2021

Accepted: 20 August 2021

Published: 2 September 2021

Publisher's Note: MDPI stays neutral with regard to jurisdictional claims in published maps and institutional affiliations.



Copyright: © 2021 by the authors. Licensee MDPI, Basel, Switzerland. This article is an open access article distributed under the terms and conditions of the Creative Commons Attribution (CC BY) license (<https://creativecommons.org/licenses/by/4.0/>).

1. Introduction

The need to reduce the aviation industry's impact on climate change and secure fuel supplies has driven investigation of sustainable aviation fuels (SAF, also referred to as "alternative fuels") for aircraft operations [1–3]. Understanding the critical impact of alternative fuel sources will provide the gas turbine industry with strategic options in sustainability and maintainability of the existing and new fleets. Over the past decade, burning alternative fuels to power gas turbine engines has attracted considerable interest and attention from the aviation industry. For instance, the feasibility of using second-generation biofuels of jatropha, algae and biobutanol was evaluated to study their effects on engine components in order to develop technologies to accommodate alloy changes.

Alternative fuels with high hydrogen/carbon ratio (H/C), such as synthetic paraffinic kerosene (SPK) produced by the Fischer–Tropsch or alcohol-to-jet (ATJ) process could produce more water vapour content than the conventional jet fuels upon combustion, and this increased water vapour level could exert a significant impact over the long-term durability on hot section components such as the substrate blades, oxidation-resistant coatings, thermal barrier coatings and environmental barrier coatings, resulting in an accelerated degradation of the turbine components. This review paper intends to identify the reaction products associated with high temperature water vapour upon burning alternative fuels, and analyzing the potential detrimental effect of these products on the hot section engine components. Potential high-temperature protective coatings that could reduce such detrimental effects are also discussed.

2. Effect of High Temperature Water Vapour on Substrate Alloys and Intermetallic Bond Coats

2.1. Effect of Water Vapour on Alloys

Ni-based superalloys have long been used as substrate blades of hot section components in gas turbine due to their better high temperature mechanical properties. Metallic bond coat has also been used to protect the substrate blade from attack of hot corrosion and oxidation. Under wet conditions during operation service, water vapor could accelerate hot corrosion and oxidation process. Marisida et al. [4] conducted a series of oxidation tests under wet conditions on substrate alloys of RENE N5, PWA 1484 alloys and Pt-modified aluminide coatings at elevated temperatures. The test results showed that oxidation is adversely affected by the increased water vapour levels, indicating that the growth of continuous and adherent alumina scale is considerably inhibited under water vapour environments, and more extensive transient oxidation occurs before the continuous α -Al₂O₃ formation takes place compared to the dry air, leading to more spinel phase formation. They suggested that, initially, the hydrogen atoms from water vapour increase cation (Al³⁺) vacancy concentration, giving rise to a rapid growth of non-protective oxide NiO, and consequently, this results in more transient oxide formation and reduces the development of continuous α -Al₂O₃ scale. They also suggested that the water vapour molecules can adversely weaken the adherence of α -Al₂O₃ scale to the alloy substrate, causing the interfacial toughness of α -Al₂O₃/alloy to decrease. It was observed that under the water vapour condition, the hydrogen changes the Al vacancy concentration, and this change favors the Ni atoms diffusion across the α -Al₂O₃ scale, leading to the spinel formation at the α -Al₂O₃-gas surface [4].

Saunders et al. [5] reviewed the effect of water vapour on the kinetics of oxide formation and growth (alumina, chromia, silica and titania) of substrate alloys and coatings. It was observed that the oxide scale morphology is affected by the presence of water vapour, probably attributed to more rapid dissociation of water vapour compared to the oxygen. It is generally believed that the water vapour promotes more porous structures in oxide scale, resulting from an increase in the cation diffusion in the scale along with consequent vacancy condensation. In the case where hydroxides or oxyhydroxides form, have higher volatility are normally observed than the corresponding oxides, leading to a loss of protection. These results demonstrate that almost all aspects concerning oxide growth such as adsorption, dissociation and diffusion of reactants are affected in the presence of water vapour compared to the dry condition. It seems that the dissociation of water on the oxide surface is more rapid at lower temperatures than at high temperature compared to oxygen. It is possible for fast diffusion of water in oxides to occur probably due to the so-called proton hopping effect, where the proton (H⁺) located at oxide ions moves by transfer from one oxygen to another. It is also known that upon the OH⁻ ion concentration being increased, there is an associated increase in cation vacancies, and this, in turn, is responsible for the observed increase in oxidation rates.

2.2. Effect of Water Vapour Effect Bond Coat

Sullivan and Mumm et al. [6] evaluated the impact of alternative fuels on hot section components of industrial gas turbine engines, focusing on the effect of alternative fuels of high-hydrogen content on the degradation mode variation via an accelerated attack of protective thermally grown oxides (TGOs) and thermal barrier coatings (TBCs). The role of water vapour levels on the volatility of TGO was carefully examined along with the water vapour transport process on the evolution of TGO and TBCs. The oxide growth behaviour of NiCoCrAlY bond coat was also examined in selected combustion environments represented by using water vapour pressure level P_{H_2O} . It was observed that the extent of spinel formation highly depends on the water vapour level during transient oxidation. The surface oxides were observed to depend considerably on the volatilization and removal of the spinels generated during the transient oxidation process. The volatilization of transient spinels from TGO surfaces was found under high water vapour environments measured through nickel volatilizing from pre-fabricated $NiAl_2O_4$ spinel pellets as a function of the combustion environment.

The vapour-phase-mediated phenomena associated with high P_{H_2O} oxidation of MCrAlX bond coat ($X = Y, Re$) was evaluated [7]. It was observed that NiCoCrAlY bond coats showed an increased non-ideal oxide formation in the TGO layer when alternative fuels are burning compared to conventional fuels, Figure 1. In this case, a continuous thin (less than $5 \mu m$) and thermo-chemically protective $\alpha-Al_2O_3$ scale may not form between the metallic bond coat and the yttria-stabilized-zirconia (YSZ) topcoat compared to burn conventional fuels; instead, a spinel-alumina bilayer develops. The formed spinel (AB_2O_4) is susceptible to cracking and delamination, and presents volume expansion between the TGO and YSZ, resulting in a weak interface with the topcoat [7]. The thick continuous spinel with $30 \mu m$ thickness shown in Figure 1 presents a significant threat to the long-term TBC durability and its life.

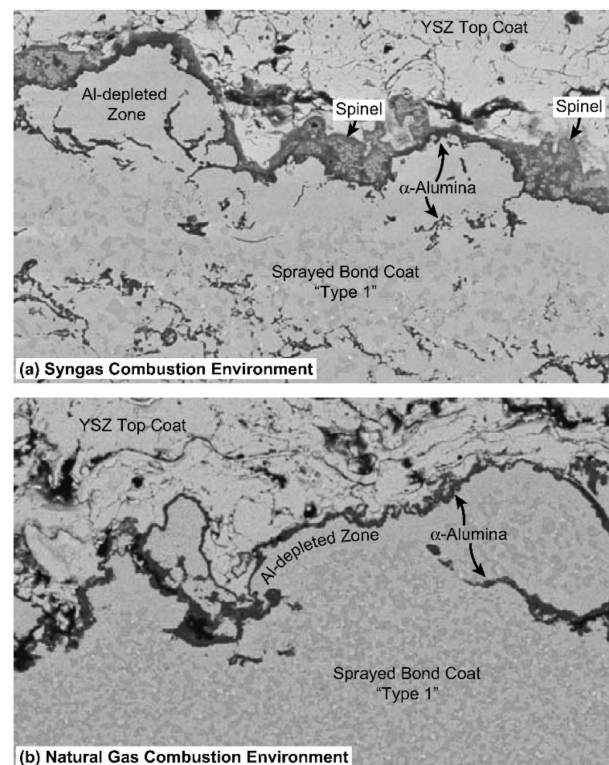


Figure 1. Images of scanning electron microscope (SEM) cross-section near thermal barrier coating (TBC)-bond coat interfaces from field tests of industrial turbine blades. Thermally grown oxide (TGO) develops dissimilarly on equivalent TBC systems when combusting (a) using syngas versus (b) using natural gas [7].

It was reported that the spinels form during the initial transient oxidation period, such as during the first several hours of high-temperature exposure period [8]. During such an initial exposure period, the oxides such as CoO, Cr₂O₃, and NiO could form and then grow first before the full formation of stable α -Al₂O₃ scale. After this initial exposure, a series of solid state reactions occur among these oxides with the stable α -Al₂O₃, this ultimately yielding (Ni, Co)(Al, Cr)₂O₄ spinels at the TGO surface [8,9]. It was identified that this transient period is normally short and the amount of spinels formed following this mechanism is often limited [10,11]. Therefore, the observed thick spinel domains with 30 μ m in size cannot be successfully explained by the mechanism proposed above.

A steady state mechanism used for a longer period was proposed by Shillington and Clarke [12] to be responsible for explaining the massive TGO spinel domains with ~100 μ m thickness exposed for over lengthy period 512 h. They suggested that as oxidation proceeds, Al content was gradually depleted in the bond coat, while the alumina scale grows thicker. Consequently, this process builds up the activity gradient for other elements in the bond coat across the TGO thickness, Ni, Co, Cr. These elements diffuse through the alumina scale, participating in spinel formation. Similarly, Maris-Sida et al. [4] postulated that water vapour could be responsible for the enhanced diffusion of divalent cation (e.g., Ni²⁺) across the TGO scale by altering the defect structure of the scale through proton incorporation. In addition, Angle et al. [13] showed that water vapor could enhance the inward diffusion of oxygen into α -Al₂O₃ scale. They suggested that proton incorporation could effectively convert O²⁻ species to OH⁻, in which their smaller size, increased polarity and the decreased charge state allow us to penetrate more deeply into the ceramic scale along the grain boundaries.

The isothermal test was also conducted to evaluate the effect of water vapour on bond coat oxidation. NiCoCrAlRe bond coat was exposed for 300 h at 1125 °C in 0%, 15%, 30% and vol. 45% H₂O vapor conditions. Continuous alumina scales are formed in all environmental test conditions and a top layer of spinel becomes thicker with increasing H₂O. At the vol. 0% H₂O condition, the spinel infrequently dots the surface, but forms a continuous layer in all wet environments higher than vol. 15% H₂O. These results are similar to that reported in the literatures showing spinel growth with increased water vapour up to 6 μ m thickness at vol. 45% H₂O [14,15]. However, Shillington and Clarke reported that spinel size can be ~100 μ m in a sample exposed for 512 h at 1121 °C [12].

NiCoCrAlY coatings were oxidized at 1000 °C for 24 h in air containing 0% and vol. 8% water vapour [15]. In all cases the surface oxides formed are alumina Al₂O₃ and CoAl₂O₄. When comparing the dry air to the moist air, much less CoAl₂O₄ was formed in moist air. The thermogravimetric data show that in the initial oxidation stage under dry, 4% and vol. 8% water vapour conditions, a typical rapid oxidation into θ -alumina occurs. This first stage is then followed by a second stage of stable oxide growth following a parabolic rate law [15]. Under the 0% and the vol. 8% water vapour, the samples experience the transition to stable growth much earlier than that under vol. 4% water vapour environment. It seems that under vol. 4% water vapour condition, the rapid growth of samples is lengthened, resulting in a greater overall mass gain due to the oxidation.

The thickness of the oxide scale formed on NiCoCrAlY was examined after being oxidized under 0–vol. 8% water vapour, and the oxide scale thickness (mostly composed of alumina) is thin around 4% upon water vapour content. While the outer spinal layer also slightly thickens around when increasing to vol. 4% water vapour, resulting in an overall combined increase in a scale thickness as water vapour content is increased. Addition of water vapour appears to increase the oxidation rate during the first stage formation of θ -alumina, then this converts to a second stable phase of α -alumina. While the first stage of oxidation rate for vol. 4% water vapour sample is increased in length, the θ -alumina is 13% less dense than that of the stable α -alumina [15]. This allows for more diffusion through the scale for a longer period of time which will allow for the transportation of more Ni and O₂ across the interface. We can conclude that the presence of water vapor will cause an increase in internal oxidation due to the increased oxygen transport across the

scale. It is important to note that vol. 4% water vapour content is the turning point for this phenomenon where the length of the diffusion path has not yet been lengthened to limit movement through the scale. Figure 2 shows an obvious trend in overall scale thickness increase as the water vapour content is increased.

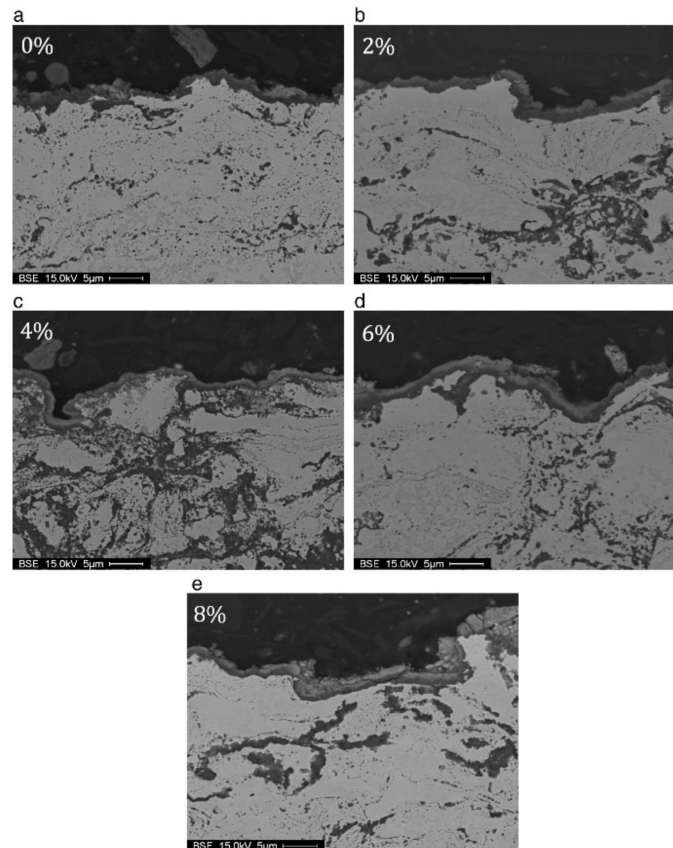


Figure 2. Backscattered electron micrographs of NiCoCrAlY coatings oxidized at 1000 °C for 24 h in air with various vol.% vapor content [15]. (a) 0 vol.%; (b) 2 vol.%; (c) 4 vol.%; (d) 6 vol.%; (e) 8 vol.%.

3. The Effect of Water Vapour on Thermal Barrier Coatings

3.1. Effect of Water Vapour on Topcoat Properties

For gas turbine engines operating under harsh environments, the hot section components of substrate blades are normally protected by high-temperature protective coatings, such as thermal barrier coatings (TBCs), to combat the heat attack and to resist oxidation/hot corrosion. TBCs are comprised of intermetallic bond coat, YSZ ceramic topcoat and thermally grown oxide (TGO) formed between the bond coat and YSZ top coat during service period [16]. The major function of the YSZ topcoat is to prevent the substrate blade from heat attack, while the intermetallic bond coat provides oxide resources to form protective TGO scale and adhesion between the YSZ topcoat and superalloy substrate. Normally the high-pressure turbine blades (HPTs) in jet engines are coated TBCs using the state-of-the-art electron beam physical vapour deposition (EB-PVD) method, in which the Pt-modified β -NiAl is used as a bond coat and fabricated by chemical vapour deposition (CVD) approaches.

As discussed, the use of high hydrogen/carbon ratio alternative fuels in jet engines increases the water vapour generation during combustion. This increased water vapour level can cause damage to gas turbine hot section components by reacting with the protective oxide scales on the component surfaces. Furthermore, the water vapour can also result in volatilization of the protective Al_2O_3 scale on the bond coat, leading to faster degradation of the coatings. According to a series of thermal cycling tests at 1100 °C under both dry oxygen or air and water vapour (10 or 50 vol.%) conditions, Haynes et al. [17] studied the

life of air plasma sprayed (APS) YSZ-TBCs on two high-velocity oxy-fuel spray processed (HVOF) NiCoCrAlY bond coats. It was found that adding 10 vol.% water vapour during the thermal cycle test reduces the TBC life by at least 20%. However, further adding 10% to 50 vol.% water vapour in the test does not lead to more reduction of the TBC lifespan. There was no clear evidence regarding the beneficial effect of adding La and Y elements to increase the TBC life, which is probably due to the low roughness ($R_a \sim 5 \mu\text{m}$) of the HVOF bond coat. It seems that the failure of TBCs does not relate to the Al depletion of the bond coat. It is interesting to note that increasing the testing cycle length from 1 h to 100 h significantly increases the TBC life under a 10 vol.% water vapour environment. The TBC's failure indicates that no obvious influence of bond coat composition, environment or substrate composition was observed on the microstructure of the bond coat and interfacial oxide scale on the failure mode of the YSZ top coating. Figures 3 and 4 show the effect of environment (dry oxygen or air + 10% vol. H_2O) and HVOF bond coat compositions on the average life of APS TBCs on alloy X4 [17].

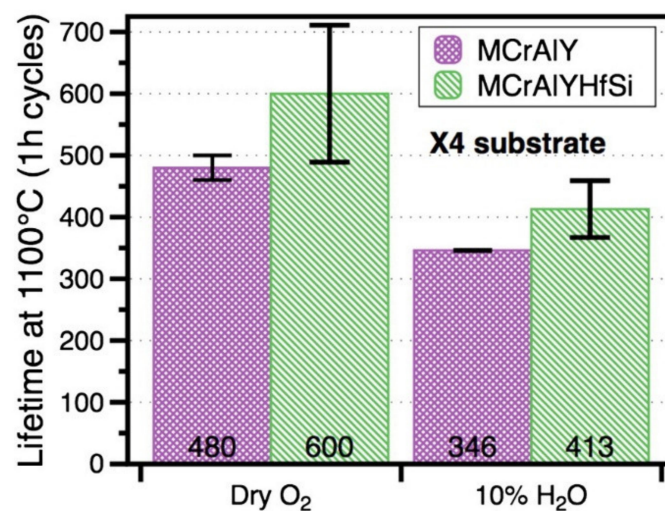


Figure 3. Comparison of the effects of the environment (dry oxygen or air + 10 vol.% H_2O) and high-velocity oxy-fuel spray processed (HVOF) bond coat composition on average air plasma sprayed (APS) TBC life of specimens on alloy X4 during 1 h furnace cycles at 1100 °C [17].

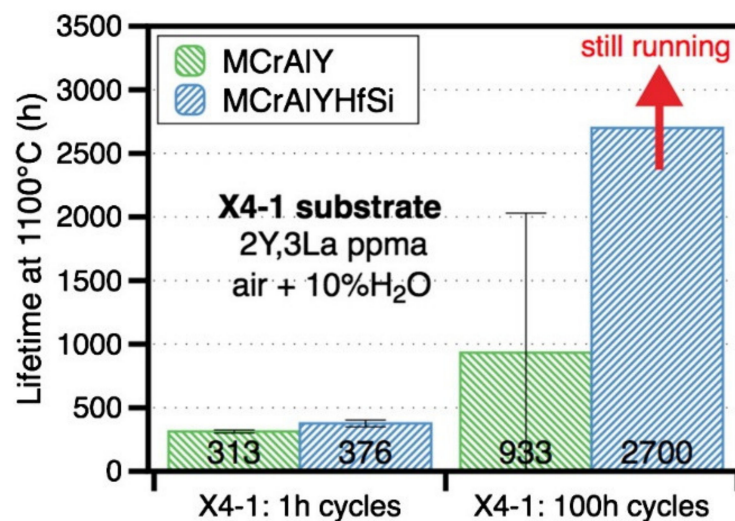


Figure 4. Comparison of the effects of cycle length (1 h vs. 100 h) and HVOF bond coat composition (NiCoCrAlY vs. NiCoCrAlYHfSi) on average time to APS TBC failure on X4-1 during 1 h furnace cycles at 1100 °C in air + 10 vol.% H_2O [17].

A 150 μm thickness of VPS NiCoCrAlY bond coat on Ni-based superalloys and 300 μm 7–9% YSZ topcoat was tested to examine the effect of water vapour on the TGO behaviour [18]. The system was oxidized in dry air, 10 vol.% water vapour, and 50 vol.% water vapour to determine its properties. Upon immersion into water vapour, the sample was analyzed for noise generation. There was a significant acoustic activity caused by the immersion which may show cracking. Although there were no macroscopic cracks observed, microscopic cracks were found during the metallographic inspection.

For samples isothermally oxidized at 1100 $^{\circ}\text{C}$ for 1200 h, the results are shown under the dry, 10 vol.%, and 50 vol.% water vapour conditions, where no cracks or delamination were identified at the time. Upon further analysis, the micrographs revealed that there was an inward growth of oxidation. The growth of the oxidation looks like in the shape of cauliflower cloud-like formations. The formation could negatively and/or positively affect the properties of the bond coat. For the positive effect, the oxide formation could increase the scale adhesion by “pegging” the oxide scale to the bond coat. For the negative effect, the inward growing oxide may penetrate through the bond coat and affect the superalloy substrate. In addition, microcracks can also be found in the 800 and 1200 h test samples but more cracks are observed in moisture than under dry environments [18].

There are other tests showing how TBCs underwent a rapid spallation when exposed to water vapour after removed from a dry furnace [19,20]. It started as a phenomenon called desktop spalling (DTS) and was later refined as moisture-induced delayed spalling (MIDS) [20] after it was confirmed that the reasons behind the spalling were the same for both theories. Similar to these findings about DTS and MIDS, it aims to highlight the effects of water vapour on the TBC when it is introduced at high temperatures in the TBC operating environment. It was already generally understood that high temperature water vapour in the operating environment shortens the lifetime of TBC coatings, but few studies look at the exact mechanisms of this early failure. An example of this shortened lifetime was investigated in [21], and from the test with the EB-PVD deposited Pt-modified aluminide coating, the introduction of H_2O in the test environment was detrimental to TBC lifetime [21].

Zhou et al. [22] conducted tests aimed to compare the behaviour of TBC properties in dry air (O_2 only) to that of moist air ($\text{O}_2 + 5 \text{ vol.}\% \text{ H}_2\text{O}$) through an isothermal furnace process at 1050 $^{\circ}\text{C}$ for durations of 200 and 400 h. The experiments were conducted on TBCs with a YSZ topcoat applied by APS, where the entire TBC has a total thickness of approximately 350 μm [22]. The SEM cross-sections of the oxides formed along the interface between bond coat and topcoat presented after isothermal oxidation at 1050 $^{\circ}\text{C}$ in pure O_2 , and in a mixture of O_2 and H_2O for 200 and 400 h, respectively. It is observed that the morphologies of the oxides formed after oxidation in O_2 were continuous and dense, whereas the oxides formed after oxidation in O_2 –5 vol.% H_2O were porous. The oxidation rate is approximately linear after 200 h [22]. This linear time period is generated by the oxide formed at the interface. This increase in oxidation can be affected by the increase in Ni and Cr cation transportation.

An X-ray diffraction (XRD) analysis was performed on the YSZ coating surface identifying tetragonal YSZ with minor amounts of cubic and monoclinic YSZ. The same phases of YSZ were found by XRD after furnace testing in both dry and moist air showing that water vapour does not react with YSZ at the experimental temperature. Zhou et al. [22] illustrated that due to the high ionic conductivity of YSZ, oxygen and water vapour can easily diffuse through the topcoat with water vapour increasing the diffusion rate, resulting in oxidation bypassing the topcoat, and occurring only at the TGO layer.

In another paper, while studying the impact of superalloy composition and bond coat roughness on TBCs, Haynes et al. [23] gathered information on YSZ topcoat spallation that took place due to oxidation at the level of the TGO in a 10 vol.% water vapour environment. In the test, they examined the specimens until a complete topcoat spallation achieved through the use of cyclic furnace testing at 1100 $^{\circ}\text{C}$ in 1-h intervals [23]. In their findings, Haynes et al. [23] found that an initial failure of the TBC usually occurred in the YSZ

topcoat where particles of alumina were found in the spalled YSZ layer [23]. These alumina particles appear to be the particles identified with white arrows in Figure 5 that are growing into the YSZ top layer. Haynes et al. also supposed that the attack on the YSZ topcoat by the alumina particles may aid in the delamination of the YSZ from the rough bond coat by providing higher stress concentrations, promoting the spalling of the YSZ topcoat [23]. Although these were the findings, Haynes et al. could not find the exact correspondence between the substrate and the spalled coating to absolutely determine the reasoning for failure. Therefore, they were unable to conclude that the alumina undercutting of the topcoat was the only reason leading to topcoat spalling.

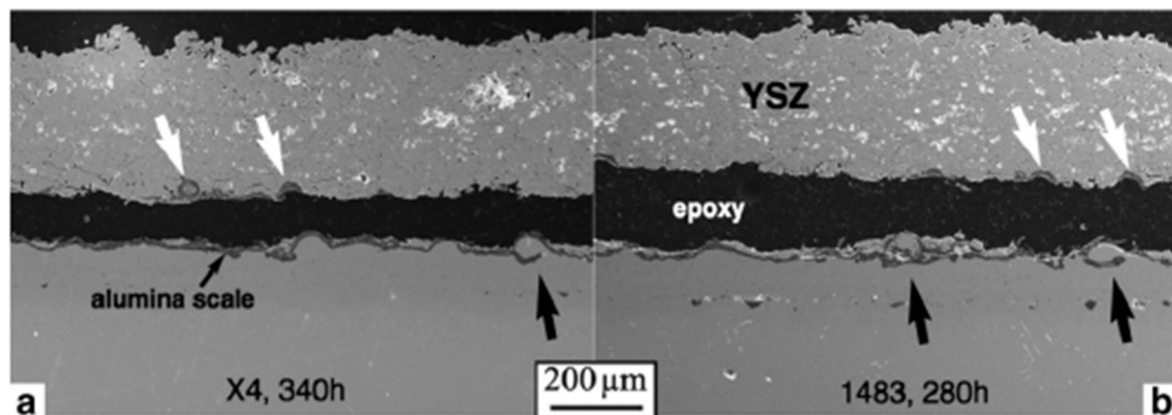


Figure 5. Scanning electron microscope (SEM) images comparing the topcoat delamination during 1-h thermal cycles at 1100 °C in 10 vol.% water vapour. (a) TBC on X4 bond coat after 340 cycles, (b) TBC on 1483 bond coat after 280 cycles. White arrows indicate alumina undercutting the yttria-stabilized-zirconia (YSZ) [23].

From the results achieved by Zhou et al. [22] and Haynes et al. [23], it seems that a YSZ topcoat of a TBC is not damaged directly by operating in an environment with high temperature water vapour. Instead, Zhou et al. found that the phases of YSZ do not change when exposed to either a dry or a humid environment, while Haynes et al. found that the spallation of the topcoat is not due to the humid environment, but due to alumina growth beneath the topcoat [22,23]. These findings show a reduction in topcoat lifetime, but not because water vapour negatively affects the topcoat directly [22]; rather, water vapour negatively affects the layers beneath the topcoat which results in topcoat spallation at a greater rate than in a dry environment [23].

3.2. Effect of Water Vapour on Crack Nucleation and Propagation

A test performed by Yanar et al. [24] on a Pt-modified aluminide bond coat covered with a YSZ topcoat applied by EB-PVD showed a significant difference in TBC durability and lifetime when comparing dry air furnace tests to the humid air furnace tests. All factors remained the same between the two tests aside from the inclusion of water vapour in the humid air tests. The results showed that the systems with water vapour above 1000 °C formed spinels (NiAl_2O_4) between the TGO-bond coat interface creating a weak path for nucleated cracks to travel through this layer to failure. It is widely agreed that TBC deterioration and eventual failure are often linked to the oxidation of the metallic bond coat at elevated temperatures via formation of a TGO layer which causes the depletion of an alloying element of the bond coat, such as aluminum [25–27].

Crack nucleation in a TBC is a gradual process, commencing from the build up of a biaxial compressive stress state at the topcoat and bond coat interface. This occurs during cooling from elevated temperatures due to a thermal expansion mismatch between the topcoat and bond coat layers [25,28]. There is a high possibility that the compressive stresses would progressively increase during thermal cycles, resulting from a reduction of deformability of the bond coat [25,29]. The biaxial stresses developed due to the thermal

expansion mismatch in the previous step could produce a residual tensile stress normal to the coating surface and/or interface at areas of local undulations. These stresses would then exert on the pre-existing defects and flaws, promoting crack nucleation and delamination in the coating system composed of oxides of $\text{Ni}(\text{Cr,Al})_2\text{O}_4$ (spinel) and NiO . These oxides are formed at temperatures >1000 °C as they are less chemically stable [25,29]. At temperatures above 1000 °C, the complex oxide layers grow rapidly, causing crack nucleation shown in Figure 6. The crack nucleation originates at the oxides of $(\text{Cr,Al})_2\text{O}_3 \cdot \text{Ni}(\text{Cr,Al})_2\text{O}_4 \cdot \text{NiO}$ and can potentially penetrate into other parts of the TBC system.

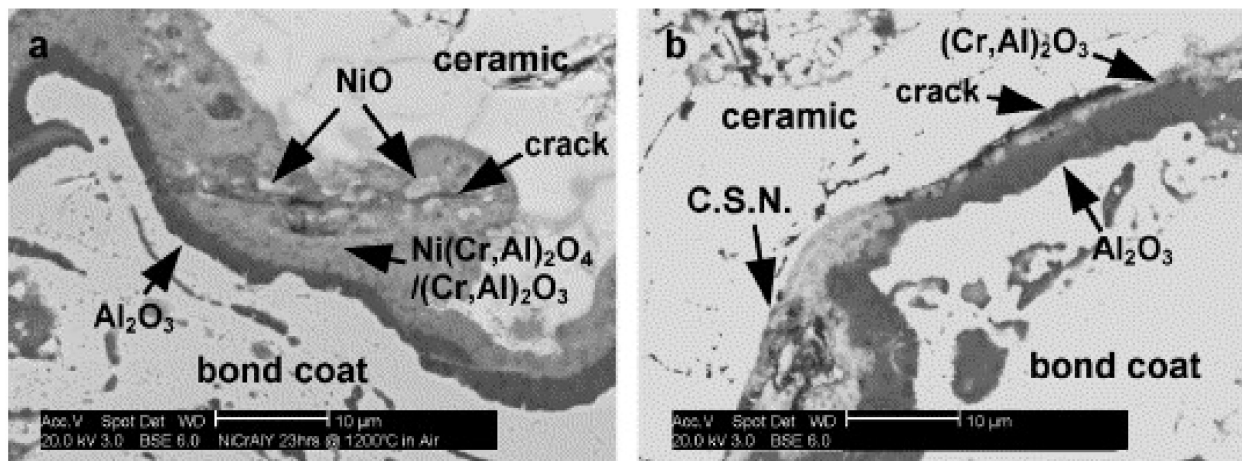


Figure 6. SEM images of crack nucleation via void formation in $(\text{Cr,Al})_2\text{O}_3 \cdot \text{Ni}(\text{Cr,Al})_2\text{O}_4 \cdot \text{NiO}$ (a), and at the interface between ceramic topcoat and $(\text{Cr,Al})_2\text{O}_3$ (b) after 23 h in air at 1200 °C [25].

An investigation conducted by Rudolphi et al. [18] was designed to identify microcracks in TBC specimens under isothermal furnace tests at 1100 °C for 200, 800 and 1200 h in dry air, air + 10 vol.% H_2O and air + 50% H_2O environments. The test was designed to capture acoustic signals generated within the TBCs when microcracking takes place. As the intensity of acoustic emissions rises, this leads to the intensity of the microcracks. The samples exposed to water vapour environment produced acoustic emissions 100 times greater than those in a dry environment, indicating that more cracking occurred when exposed to water vapour. These acoustic emissions did not change significantly between the tests with 10% H_2O or 50 vol.% H_2O , suggesting that cracks occur more readily in a humid environment, but not more or less depending on the amount of water vapour in the environment [18]. Upon further examination using optical micrography of 800 and 1200 h samples, Rudolphi et al. observed that microcracking occurs slightly more often in the water vapour environments, but would need to obtain more sample tests before a firm conclusion can be drawn. From these micrographs, Rudolphi et al. were then able to find that the majority of the microcracks were formed on the YSZ-side of the TGO layer with cracks penetrating the interface [18]. Although these cracks are not in the YSZ layer, they may eventually promote early spallation of the topcoat, shortening the usable TBC lifetime.

The turbine exhaust from the combustion zone of a gas turbine engine can be expected to be 12–14 vol.% in water vapour content when burning natural gas and up to 15–30 vol.% for burning high hydrogen fuels [7]. Water vapour can significantly alter the oxidation rate, microstructures and corrosion resistance of the thermally grown oxide (TGO) in TBCs, which in turn reduces the lifespan of the system [7,30,31]. The exact mechanisms by which water vapour affect TGO performance are not fully understood [28]. A comparison of TGO behaviour in different superalloys in wet and dry air was made, where the experiments were conducted under 10 vol.% H_2O wet air [7,30,31]. The presence of water vapour has been found to alter the phase transformation rate of the growing alumina scale [30], promoting the growth of metastable or transition alumina ($\gamma\text{-Al}_2\text{O}_3$, $\delta\text{-Al}_2\text{O}_3$, or $\theta\text{-Al}_2\text{O}_3$) in $\beta\text{-NiAl}$ bond coats [32].

Lance et al. [28] observed a higher content of θ - Al_2O_3 grown on Pt-modified alumina bond coatings after 1 h at 1125 °C and 1150 °C tests in 10 vol.% H_2O air. The presence of water vapour accelerated the growth rate of the alumina scale. Under dry and wet air, the oxidation process follows the parabolic rate law. However, under $\text{H}_2/10$ vol.% H_2O , the parabolic rate constant is larger, leading to a faster oxidation rate [29]. The water vapour is suggested to stabilize the faster growing metastable θ - Al_2O_3 phase resulting in a thicker TGO compared to scales grown in dry air [28]. Chromia scales were also found to grow at significantly faster rates in the presence of water vapour. Fontana et al. [29] observed a 25% mass increase for uncoated Crofer22 APU oxidized in $\text{O}_2/10$ vol.% H_2O at 800 °C compared to the scale mass grown in dry air.

According to Ref. [28], the introduction of Pt into the TBC increased the lifetime significantly at 1125 °C and 1150 °C for the N515 and the N5 samples, respectively. When comparing the average difference in lifetime of the tested samples at 1150 °C and 1125 °C, one finds that the increase in temperature by only 25 °C largely lowers the lifetime of all test samples by four times. Comparing the average lifetime of the samples with identical substrates such as the N5 and the X4 tested with and without the presence of water vapour, one can observe a drop of about 50% in TBC lifetime.

Using the Wyko system, the surface roughness of the test samples was measured to identify the effect of water vapour. As expected, the addition of 10% vol. water vapor increases the surface roughness after thermal cycling of all test samples with the exception of X4 substrate with Ni(Pt)Al coating. This X4 sample decreased in roughness with the addition of 10% water vapour, which is of particular interest because the increase in surface roughness is an indication of an onset coating failure. One possible reason why the N515 substrate material did not increase in roughness to the same degree as the other samples could be due to the higher Hf content in the N515 (Hf of 0.2%) while for N5 samples, Hf content is only 0.05%, with the X4 samples being 0.03 % [33]. It has been summarized from these studies that Hf content exerts a positive effect on lowering surface roughness of the test samples [28].

When exposed to dry air, alumina-forming bond coats oxidize to create a uniform, thermochemically protective α - Al_2O_3 scale on the order of around 5 μm [7]. The α - Al_2O_3 scale can be thought as being dehydrated because as the temperature rises water is driven out of the structure's interstitial sites. Higher water vapour content means that more time is required to remove the water from the scale's structure allowing for the prolonged existence of γ , δ , and θ phases. The temporary stabilization of the γ and δ -alumina phases in the presence of water promotes diffusion of Cr, Co, and Ni cations from the substrate to the TGO interface. The solid state reaction of these oxides with the alumina form spinel [7]. The brittle whisker-like spinel is associated with the reduced TGO life [29].

The spinel shows brittle characteristic and is more prone to cracking. This structure also results in volume expansion when formed, thus weakening the TGO and topcoat interface. Sullivan et al. [7] observed spinel formed on the order of 30 μm in thickness. The larger the spinel, the less stable the TBC will be over the course of thermal cycling. In all cases, water vapour content was found to significantly reduce corrosion resistance in both chromia and alumina TGOs [30,31]. The amount of spinelling observed in TGO is directly related to the water vapour content in the air. Figure 7 illustrates how an increase in spinel and NiO coverage of the substrate after thermal loading increases with water vapour percentage. Initial alloy phases with large amounts of Ni, Co, and or Cr produce oxide products that contain a large quantity of those elements as well. From the comparison of (a), (b), and (c) to (d), (e), and (f), it is shown that the high Al β -phase becomes α - Al_2O_3 , the low Al γ -phase becomes α - Al_2O_3 with spinel, and the M, Y-rich phases become areas of NiO encircled by spinel [7]. As the water content increases, the amounts of unwanted oxides increase until at 15 vol.% H_2O the surface is almost completely covered in spinel and NiO.

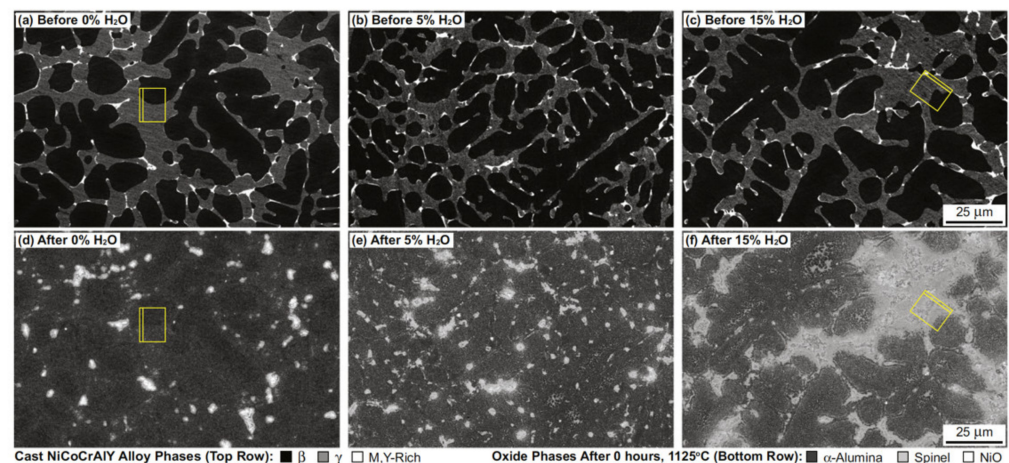


Figure 7. Before and after SEM images of cast NiCoCrAlY TGO grown in 0 vol.% H₂O (a) and (d), 5 vol.% H₂O (b) and (e), and 15 vol.% H₂O (c) and (f) after thermal cycling at 1125 °C [7].

The surface coverage of spinel increases with water vapour percentage before reaching a plateau around 15–30% vol. H₂O and then falls slightly after 50 vol.% H₂O which was the highest value tested by Sullivan et al. [7]. For chromia scales, the grain size of the TGO is reduced with the presence of water, and this may increase plasticity and relieve stress in the TGO layer which helps to prevent local cracking [29]. The effect of water vapour on chromia and alumina scales does not appear to be the same. For chromia scales, water improves the adhesion at the alloy–scale interface delaying spallation compared to the samples in dry air which showed severe buckling under cyclic oxidation at 950 °C [29]. However, although the scale was less prone to spall, the oxide formed on the surface of the alloy was more porous and less protective of the substrate [29]. In alumina-forming TGOs, water increases scale spallation [30,34].

The promotion of spinel roughens the surface of the TGO, and air with 10 vol.% water vapour results in a 0–7% increase in TGO surface roughness compared to the scales formed in dry air. Lance et al. [28] explained that the Keyence roughness is lower than the Wyko roughness as it was taken at a comparatively low magnification (500×) to match other measurement techniques used in the paper [28]. Both chromia and alumina scales saw minimal changes in TGO residual stress between dry and wet air samples after prolonged cyclic oxidation [30,31].

According to the analysis above, it can be said that high-temperature water vapour negatively affects TBC behaviour, as TBC lifetime tends to be reduced under high temperature water vapour environments. As TBCs comprised layers of different compounds, water vapour impacts the TBC differently at each scale. Results from Zhou et al. [22] and Haynes et al. [23] could not reach the conclusion that water vapour directly affects the TBC topcoat in a negative manner. Instead, it was suggested that oxygen and H₂O can diffuse through the topcoat, resulting in the oxidation of the bond coat. Zhou et al. [22] illustrated that due to the high ionic conductivity of water, the rate of this oxidation of the bond coat is increased with the inclusion of water vapour in the operating environment. Haynes et al. [23] observed that the initial TBC failure occurred in the YSZ topcoat. Within the topcoat failed, SEM images showed particles of alumina had grown into the topcoat, decreasing its structural integrity while increasing regions of stress concentration, ultimately leading to the failure of the top coat.

In a study to observe cracking of TBCs in dry and wet air conditions, Yanar et al. [24] found crack nucleation and propagation between the topcoat and TGO interface. This weak path allowed for easy crack propagation and eventual failure of the TBC. However, Yanar et al. [24] did not observe crack propagation into the topcoat. Another study conducted by Rudolphi et al. [18] was trying to study microcracks in a YSZ topcoat during the isothermal furnace tests with varying levels of humidity. During these tests, the sound

emitted from the samples exposed to a humid environment was much greater than those exposed to a dry environment. This suggests that YSZ topcoats are more prone to cracking in humid environments. It should be noted, however, that during these isothermal tests, no macrocracks were identified in the samples. Upon further inspection, Rudolphi et al. [18] found that microcracks were more prominent in the humid samples but would have to generate a larger sample size in order to make a statistically conclusion. With cyclic furnace tests, these microcracks may be able to grow to macrocracks and reach a size that may be detrimental to the TBC.

3.3. Effect of Water Vapor on TGO

Finally, the effect of high temperature water vapour on TGO layer was identified. This layer appears to be the most affected by H₂O in the TBC operating environment. It has been found that the TGO scale undergoes faster oxidation in wet air conditions than in dry air conditions, leading to a thicker TGO layer. Furthermore, when grown in dry air, a uniform α -Al₂O₃ is formed. Wet air conditions prolong the existence of γ , δ , and θ phases of the oxides. The temporary stabilization of these phases promotes the growth of unwanted oxides which form spinel and could promote crack nucleation and propagation. Additionally, the spinel is also thick, creating stress concentrations on both top coat and bond coat, reducing TBC integrity over repeated thermal cycles. The amount of spinelling in the TGO is a direct result of the amount of water vapour in the environment with a growing amount of unwanted oxides forming until the environment is 15 vol.% H₂O. When the environment reaches this level of humidity, the TGO surface is entirely covered by unwanted spinel and NiO. The spinel formed due to the water vapour environment roughens the surface of the TGO when compared to the oxide grown in a dry environment.

The effect of water vapour on chromia scales appears to be different from that on alumina scales. The presence of water vapor reduces the grain size of the TGO, increasing plasticity and relieving stress. Chromia test samples appeared to have better adhesion to the alloy, delaying spallation when compared to alumina scales under the same testing conditions. Unfortunately, the chromia scale appeared to be more porous and less protective of the underlying substrate when it was exposed to the wet air environment. Both the chromia and alumina scales saw minimal changes in TGO residual stresses between dry and wet air samples after prolonged cyclic oxidation.

The lifetime for Pt diffusion bond coats was studied in varying water vapour concentrations. The EB-PVD YSZ-coated samples were measured for lifetime at 1150 °C after 1 h cycles. Two different Pt bond coats were used, Pt-modified β -NiAl and a $\gamma + \gamma'$ Pt diffusion coats. For the Pt-modified β -NiAl bond coat, the water vapour has a much larger effect than it does on the Pt-diffusion $\gamma + \gamma'$ coat. The β -NiAl coating lifetime expectancy was reduced inversely compared to the water concentration. The β -NiAl coating results can be explained in terms of the rumpling of the bond coat. The increase of lifetime in N515 base alloy is due to the higher amount of Hf in the alloy. For the $\gamma + \gamma'$ coating on the N515, the high Hf amount in the alloy caused deep internal oxidation. This oxidation is primarily composed of alumina and oxide particles with high amounts of Hf [35].

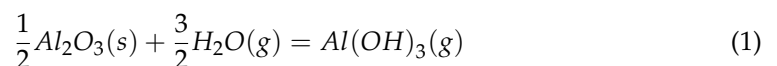
The cross sections of a TBC-YSZ with Pt modified β -NiAl as bond coat were examined [36]. These sections are taken from samples after failure during the 1 h cycle test at 1150 °C. The bottom of the sections displays the specimen without the YSZ layer, while the top shows the opposite side with the bond coat beneath the YSZ layer. The constriction of the YSZ layer on the top side seems to reduce the rumpling. Under the 90% water vapour condition, there are γ' layers within the coating/substrate interface as well as at the gas interface. On these areas, the interdiffusion caused transformation results in a phase from high aluminum β -NiAl to the low aluminium γ' [36]. Rumpling that was found in the Pt-modified NiAl bond coat is caused the β - γ' transformation through interdiffusion. The internal oxidation is supported by other studies as well [21].

Experimentation has also shown that the presence of water vapor can alter the corrosion rate. Testing samples in an environment hosting a 5–15 vol.% water vapor content

at 800–1100 °C can increase the oxidation rate in some compositions of substrate and top-coat [14,37–39]. The composition of the materials that experienced this had NiO, Cr₂O₃ and Ni(AlCr)₂O₄ increase with water vapour. The oxide scale produced was more porous, and an earlier onset of oxide spallation due to the presence of the water vapor occurs [37,40].

For the formation of main oxide alumina, the possible mechanism to accelerate the corrosion rate will be water-assisted cracking during thermal cycling. However, this could not be a sufficient reason to cause an early failure in this case. The experiment concluded that as long as the following is true then the presence of water vapor should have little to no effect on oxide growth: (1) coatings form alumina scale with strong adhesion (Y, Ta, Si or low sulfur coatings); (2) coatings form mainly alumina. When the non-TBC coated and TBC coated samples were evaluated, the experiments concluded that both showed similar corrosion attack. The TBC coated samples did not develop porosity in the bond coat or the substrate [37]. It should be noted that this experiment was performed at a much lower temperature and for longer time durations on average than what is typically in the literature. There are a few characteristics of the test results that should keep this into account. The most other experiments saw large decreases in oxidation and TBC life by increasing the testing temperature by even 25 °C, which the average temperature for the reviewed literature being about 1000 °C. This lower temperature could be a factor as to why the action of the water vapour had little to no effect on the oxidation and TBC life in this particular experiment.

It was known that the alumina is frequently used as a protective oxide scale for many coatings. The stability of Al₂O₃ scale varies when subjected to water vapour at high temperatures. The alumina instability is caused by the aluminum hydroxide formation as shown below,



One of the principal mechanisms that causes the failure of the coating is the development of holes and cracks or the cracking off of the alumina layer. In dry air, the Al₂O₃ scale was subjected to large strains and fluctuations during the oxidation cycles. These fluctuations cause stress concentrations in rumples in the form of tensile forces at the peak and compressive stresses at the troughs of the layer. Due to the low oxidation lifetime in air containing water vapor, the created stress is non-uniform and once it exceeds the fracture stress, the alumina will crack and fall off [41].

4. Effect of Water Vapor on Environmental Barrier Coatings (EBCs)

The high-temperature capability of the current hot-section components of gas turbine engines could reach its limit, and any further improvement of the inlet-temperature becomes significant challenge. The application of ceramic thermal barrier coatings (TBCs) along with the internal air-cooling system in blades has resulted in higher inlet-temperatures in gas-turbine engines [42,43]. During this process in withstanding the higher inlet-temperature, the silicon-based ceramics leads to a jump in temperature capability.

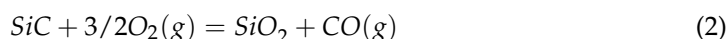
Silicon-based ceramics, such as ceramics matrix composites (CMCs), are important materials for turbine engine hot sections due to their capabilities of withstanding hotter temperature, their excellent mechanical and physical properties and lower density than other alternative metals/alloys. Their utilization imparts various benefits of utilizing ceramic hot section components, that embody weight reduction in engine parts, and improved rotary engine potency similarly as the generation of increased power output and lower emissions due to reducing or eliminating cooling in areas of the rotary engines. Potential turbine ceramic parts for industrial, commercial, and/or military high-temperature rotary engine applications embody combustor liners, vanes, rotors, rotary engine frame flow path, and shrouds. These parts need materials that may withstand high temperatures and pressures for a long duration in a steam-rich environment.

SiC-based CMCs endure active chemical reaction and degradation within the high-temperature, high-pressure and high-velocity gas stream of the gas-turbine engine that

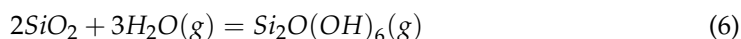
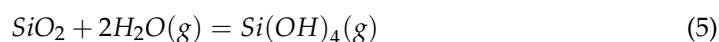
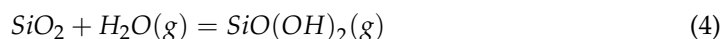
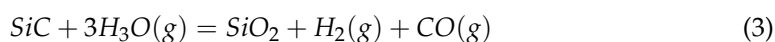
invariably contains water vapors produced as a by-product of fuel combustion. For turbine engines to operate safely and efficiently, they need to have dense, and crack-free environmental barrier coatings (EBCs) to shield SiC-based CMCs from this environmental attack by obstruction diffusion/ingression of oxygen/steam [42–44]. To achieve crack-free EBCs, a high coefficient of thermal growth (CTE) is required to match SiC-based CMCs substrates; however, this limits the selection of available ceramics as EBCs [45,46]. In addition, EBCs should have low volatility to minimize steam-induced corrosion/recession and be immune to degradation by liquefied calcia-magnesia-aluminosilicate (ingested dirt, sand, or ash; usually mentioned as CMAS) deposits, among many different necessities, together with high-temperature capability; part stability; chemical compatibility with different layers; and mechanical strength (high hardness and toughness) against fracture, erosion, and impact-damage [43,45,46]. Since the failure of EBCs can result in the degradation of CMCs, EBCs need to be designed highly reliable.

4.1. Water Vapour Reaction with Thermally Grown Oxides (TGO) Scale

Investigations have demonstrated that at higher temperatures in a dry oxygen environment, SiC CMCs have excellent oxidation resistance due to a strong and moderate silica scale. In this case, this silica scale responds with water vapor, a by-product of combustion responses and develops a gaseous silicon hydroxide. In dry oxygen conditions, SiC reacts with oxygen to form a protective silica SiO_2 scale [47],



Similarly, SiC can react with water vapor to form silica. However, the formed silica scale can further react with the water vapour, according to Equations (3)–(6), to form silicon hydroxide or silicon oxyhydroxide which are volatile in nature, and results in the loss of environmental protection [48], which is known as surface recession,



The ensuing simultaneous oxidation and surface recession can produce a porous silica scale. These porous scales provide easy paths for oxidant to diffuse to the SiC/SiC-CMC substrate. Figure 8 illustrates schematically the oxidation, surface recession and porosity formation when the SiC/SiC-CMC substrate is in contact with high-temperature combustion gases [49].

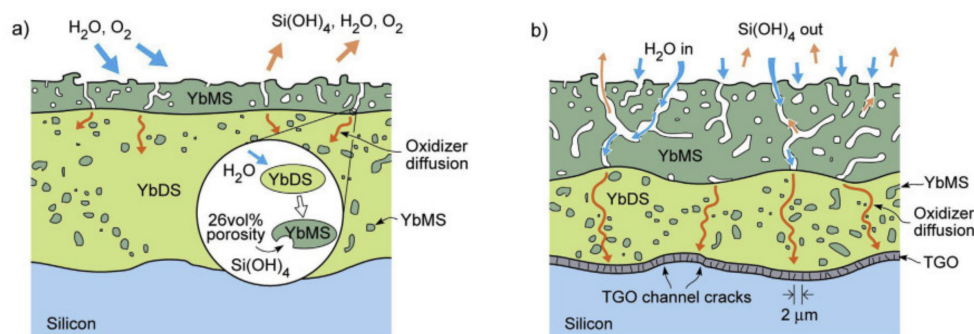


Figure 8. Schematic show of silica TGO volatilization and formation of porous ytterbium monosilicate layer (YbMS) on ytterbium disilicate (YbDS) surface, and TGO layer on silicon bond coat after steam cycling. (a) Early stage of volatilization, and (b) late stage exposure process, where microcracked TGO is presented [49].

The high recession rates of SiC-based substrates via silica volatilization induce a significant degradation of SiC CMCs. Therefore, an oxide more thermochemically stable than the SiO₂ scale must be applied as an environmental barrier coating (EBC) to guard SiC CMCs from high-temperature water vapor attack [50].

EBCs have been applied to reducing/minimizing such surface recession of SiC/SiC-CMC substrate from combustion gases including water vapor attack. As demonstrated before, due to the high H/C ratio of alternative fuels, high-temperature water vapour will be produced upon burning these fuels. These EBCs appear to be effective in inhibiting water vapour volatilization of TGO SiO₂ scale [51].

To effectively protect the CMC (SiC_f/SiC_m) substrate from water vapour attack, EBCs are normally made with high density such that no more open pores and cracks allow the water vapour to penetrate the EBC topcoat and reach with the CMC substrate. Currently, a number of types of EBC have been developed, for example, a multilayered Si/mullite + BSAS (barium-strontium-aluminum-silicate)/ScSiO₅ EBC for SiC/SiC CMC vane [48]. The Si bond coat was deposited on SiC/SiC substrate, whereas the mullite + BSAS layer is applied to improving the crack resistance of the EBC layer. The temperature capability of CMC is higher than the BSAS thermal stability limit; therefore, to work at an even higher temperatures, coatings with high-temperature capability are required along with low thermal conductivity. It was already demonstrated that EBC is used to protect the CMC substrate from the water vapour-induced hot corrosion, meanwhile, developing a high-temperature thermal/EBC (T/EBC) system would need coatings that consist of a high-temperature ceramic layer, such as a zirconia-based three-layer BSAS EBC system [51]. Furthermore, a transition layer is necessarily needed, in which this transition layer has an intermediate coefficient of thermal expansion (CTE) capable of accommodating the CTE mismatch between the BSAS layer (about 5 ppm/°C) and the topcoat layer (about 10 ppm/°C in the case of stabilized zirconia). Consequently, the design will have a multi-layer system that presents significant challenges regarding fabrication processing, thickness requirements and the cost.

4.2. Surface Cracking due to Water Vapour

Cracking on the surface is often observed and a primary concern in high-temperature protective coatings. Although surface cracking modes have been studied extensively in TBCs [52], more work is needed in EBCs regarding the cracking mode identification. Through-thickness cracks are frequently seen in TBCs; such cracking can affect interface delamination of coatings, and this was less researched for EBCs. Thermal stress and residual stress disseminations in EBCs were mathematically examined considering the impacts of topcoat morphology. Inclinations of crack redirection and delamination in EBCs were assessed as the capacity of function of death in various layers and material properties by figuring energy discharge rates, individually. Damage because of thermal stresses was concentrated by reformist disappointment examinations utilizing most extreme stress criterion [49].

As shown in Figure 9 [53], the cracking on the surface, the topcoat layer variation and TGO scale growth occur during the high temperature water vapor attack. Initially, no cracks appear in the EBC system in which pure ytterbium disilicate (YbDS) as topcoat while Si as bond coat. Upon the upper part of YbDS converted into an ytterbium monosilicate layer (YbMS) during hot steam cycling, cracking on the surface was initiated during the ensuing cooling stage because of thermal stresses. In the early stage of steam cycling, the propagation of a surface crack runs along YbMS layer, suggesting that cracks are driven by stresses due to CTE mismatch of YbMS. Accordingly, material change in the topcoat instigated due to volatilization by water vapour was the prevailing component in the early stage. With the volatilization and oxidation, the surface cracks propagate toward the interface due to YbMS layer in the topcoat. Meanwhile, TGO grows during the initial 2000 h. In this case, parabolic growth of TGO became obvious subsequently, because of the restricted oxygen hindrance impact of the permeable YbMS layer and the diminishing

thickness of the residual YbDS layer. Because of TGO growth, the stress due to oxidation accumulated continuously, and at the point when the TGO thickness arrived at a critical value, $\sim 4 \mu\text{m}$ for this situation, the oxidation stress was adequately large to drive further propagation of the surface cracks. Thus, the entire topcoat, counting the YbMS surface layer and the residual YbDS layer, was entered in a moderately brief timeframe while the YbMS thickness was practically unaltered. After the catastrophic penetration, the through-thickness surface crack could give an alternate route for quicker oxygen dissemination and prompt inhomogeneous TGO growth after infiltration.

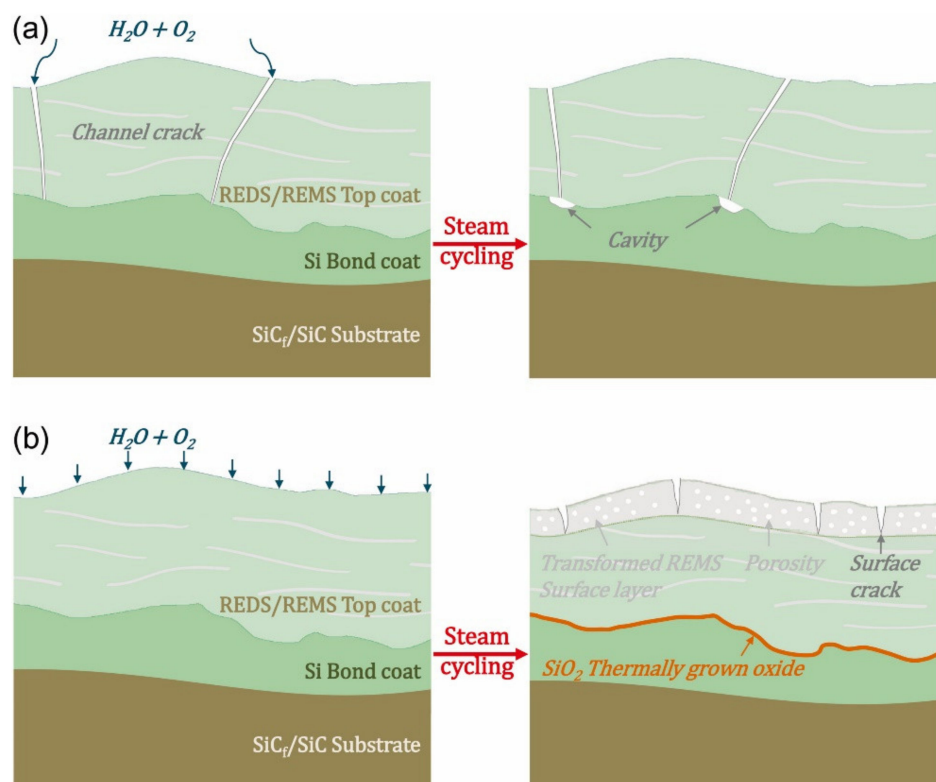


Figure 9. (a) Premature failure via interface delamination through channel cracks; (b) intrinsic failure via coating spallation at topcoat surface [53].

4.3. Recession of Environmental Barrier Coatings

Using a high-pressure burner rig, Robinson et al. [54] studied the SiC recession behaviour induced by SiO₂ scale volatility under combustion conditions to simulate gas turbine combustion. Normally, the linear weight loss and surface recession rates for SiC were observed in both fuel-lean and fuel-rich gas mixture conditions. The effect of pressure and gas velocity on recession rates was examined during a gaseous-diffusion-controlled process for volatile reaction products such as SiO, Si(OH)₄, and Si(OH)_x. It was identified that the oxidation process follows the parabolic kinetics, and linear volatilization rates were measured. Increasing the testing temperature can accelerate SiO₂ volatility rate, and based on a fitted Arrhenius correlation, the volatility increases with both pressure and velocity, thus lending support to a chemical mechanism based on a Si(OH)₄ volatile species. Under typical combustion conditions, the recession rates of 0.2–2 $\mu\text{m}/\text{h}$ were predicted between 1200 °C and 1400 °C. Thus, it is concluded that a long-term, high-temperature and high-velocity exposure could degrade significantly silicon-based or SiO₂-forming coatings by water vapour recession in combustion gas environments. Therefore, high-temperature protective coatings are needed for SiC or other silicon-based materials in combustion containing H₂ or H₂O.

A variation of the oxidation rate of silicon carbide was examined [55] versus the water vapour pressure. The CVD-SiC was oxidized between 1000–1400 °C under H₂O/O₂

mixtures in 10–90 vol.% water vapour at total pressure 1 atm. Water vapour has been demonstrated to increase the oxidation rate of SiC between 1100–1400 °C by an order of the magnitude over the rates observed in oxygen. The power-law rate for parabolic oxidation in the water vapour partial pressure at high temperatures showed that the molecular species were not the sole rate-limiting oxidant. These results can be well described by a model, where the diffusion of molecular H₂O and a charged species, such as OH[−], both determine the oxidation rate of SiC. Variation regarding the oxidation mechanisms and morphologies prohibits the exact determination of activation energy for oxidation.

By using both the high-pressure burner rig (HPBR) and water vapour cyclic furnace, the recession behaviour of uncoated, mullite-coated and mullite/YSZ-coated SiC was examined by Lee [56], where the remaining samples were exposed under a rich fuel burn condition (~equivalence ratio 51.9). At the pressure of 6 atm and temperature of 1230 °C, the uncoated and mullite-coated SiC illustrated a weight loss resulting from the volatilization of silica scale. In contrast, the lack of weight change in the mullite/YSZ-coated SiC demonstrated that the YSZ overlay coating is capable of protecting coating from water vapour attack. In addition, the enhanced oxidation behaviour was observed around pores, indicating that water vapour has penetrated the cracks and reacted with SiC. The weight loss of mullite-coated SiC/SiC was due to the selective volatilization of silica from the mullite.

Zhu et al. [51] explored the failure mechanisms of thermal and environmental barrier coating systems tested under cyclic thermal gradient conditions. Plasma-sprayed ZrO₂-8 wt.%Y₂O₃ and mullite + BSAS/Si multilayer thermal and environmental barrier coating (TBC-EBC) systems coated on SiC/SiC substrates were thermally cycled under high thermal gradients using a laser high-heat-flux rig in water-vapour environments. It was observed that the water vapour facilitated the initial thermal conductivity increase of topcoat that originated from the enhanced sintering and interface reaction, and then late promoted conductivity reduction due to the accelerated coating cracking and delamination.

Lee et al. [45] studied the volatilization behaviour of topcoats by thermogravimetric analysis (TGA) of hot-pressed monolithic EBC coupons. The TGA was obtained for the tests in a 50 vol.% H₂O–50 vol.% O₂ environment flowing at 4.4 cm/s under 1 total atm pressure at 1500 °C. EBC performance was evaluated via thermal cycling in simulated lean combustion environments. All EBC-coated test coupons were initially annealed in the air at 1300 °C for 20 h before starting test to stabilize coating phases. It was noted that most thermal cycling tests were conducted at 1300 °C (or 1316 °C) and 1380 °C under 90 vol.% H₂O-balance O₂, flowing at 2.2 cm/s under 1 total atm pressure by using automated thermal cycling furnaces. The purpose of choosing 1380 °C as the upper test temperature, instead of 1400 °C, at the topcoat/intermediate coat interface, was to avoid an accidental melting of the Si bond coat, whose melting point is 1416 °C for pure Si which is lower when contaminated.

Figure 10 plots the weight change with respect to time for hot-pressed BSAS family materials exposed to 50 vol.% H₂O-balance O₂ flowing at 4.4 cm/s at 1500 °C and 1 atm total pressure. It was observed that BAS (BaO-Al₂O₃-2SiO₂) illustrates the highest volatility, followed by SAS (SrO-Al₂O₃-2SiO₂) and then BSAS. The volatility and the associated recession rates at higher flow rates and high pressures experienced in actual gas turbines can be described via a silica volatility model [48] along with using the volatility data from Figure 10.

In Figure 11a,b, the weight changes versus time are plotted for selected hot-pressed rare earth silicates exposed to 50 vol.% H₂O balance O₂ flowing at 4.4 cm/s at 1500 °C under 1 atm total pressure. The volatility data of BSAS is also included in Figure 11 for comparison. The rare earth oxide and silica were mixed in a specific ratio to produce rare earth monosilicates upon being completely reacted. The weight change of Yb₂SiO₅ and Er₂SiO₅ remained reasonably flat pattern, while Y₂SiO₅ and Lu₂SiO₅ showed a slight weight gain and Sc₂Si₂O₇ + Sc₂O₃ showed a small weight loss.

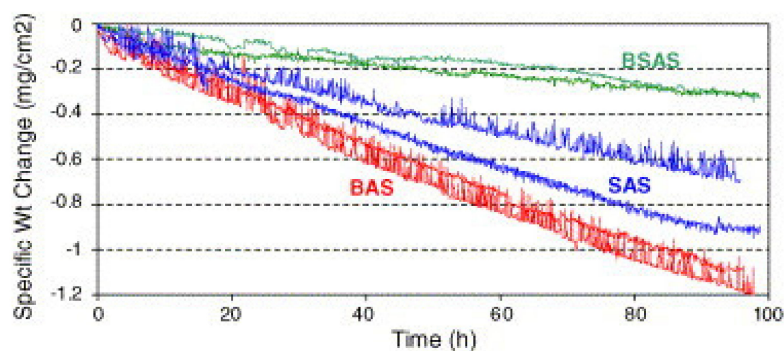


Figure 10. Volatility of hot-pressed BSAS (barium-strontium-aluminum-silicate) family materials exposed to 50 vol.% H₂O-balance O₂ flowing at 4.4 cm/s at 1500 °C and 1 atm total pressure [45].

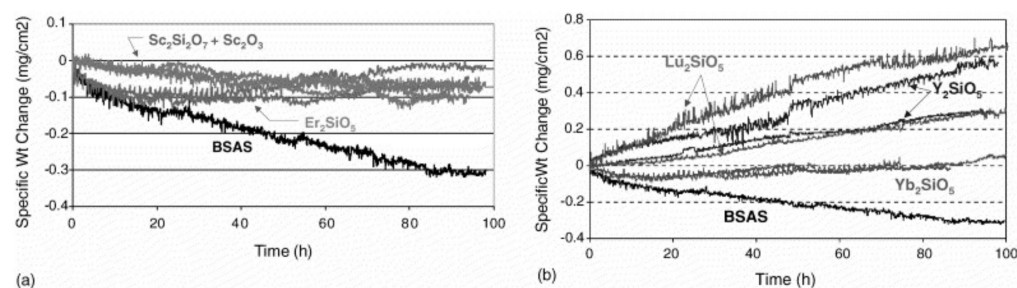
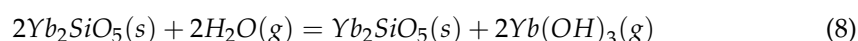
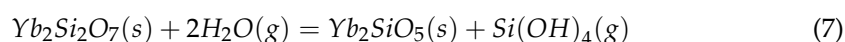


Figure 11. Volatility of hot-pressed rare earth silicates exposed to 50 vol.% H₂O-balance O₂ flowing at 4.4 cm/s at 1500 °C and 1 atm total pressure [45]. (a) weight change versus time for rare earth Sc₂Si₂O₇ + Sc₂O₃, Er₂SiO₅ and BSAS; and (b). weight change versus time for rare earth Lu₂SiO₅, Y₂SiO₅, Yb₂SiO₅ and BSAS.

Initially, Ueno et al. [57] performed a series of water vapour corrosion resistance tests on selected monolithic oxides of Al₂O₃, HfO₂, TiO₂, ZrO₂, Al₆Si₂O₁₃, Al₂TiO₅, Lu₄Hf₃O₁₂, Ln₂Si₂O₇ (Ln = Yb and Er) and mullite/Lu₂Si₂O₇ eutectic bulk at above 1300 °C. They found that HfO₂ and ZrO₂ illustrate a better corrosion resistance to water vapour at elevated temperatures. Among low-thermal-expansion oxides, Lu₂Si₂O₇ illustrates a better corrosion test's weight loss rate, in which these oxides also show a coefficient of thermal expansion close to silicon nitride. For polycrystalline Lu₂Si₂O₇, the grain boundary silica was found to be prone to water vapour corrosion. It was also observed that without boundary silica, the corrosion resistance of Lu₂Si₂O₇/mullite eutectic bulk phase was better than the polycrystalline Lu₂Si₂O₇ bulk phase.

Ueno et al. [58] also examined the recession behaviour of Yb₂Si₂O₇ under high-speed steam jet at high temperatures. They demonstrated that the recession mechanism for Yb₂Si₂O₇ phase is due to the decomposition of Yb₂Si₂O₇ phase associated with the corrosion of silica component following Equation (7) that occurs above 1300 °C. The silica component was then removed by water vapour, and polycrystalline Yb₂SiO₅ phase was generated within the interior grain of Yb₂Si₂O₇. Based on Equation (8), the recession also occurs above 1300 °C even if the recession from Equation (7) is dominant up to a 1400 °C test. Porous structures were formed on the surface due to corrosion of silica component and recession of boundary phase above 1400 °C. Surface cracks are generated due to the volume reduction and subsequent tensile stress was developed during the decomposition of the Yb₂Si₂O₇ phase at 1400 °C. The recession based on Equation (8) is dominant at 1500 °C.

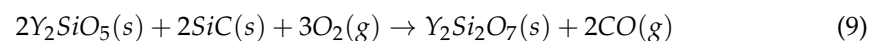


Richards et al. [49] carried out tests on ytterbium disilicate environmental barrier coatings under thermal cycling in water vapour conditions. The EBC system was designed

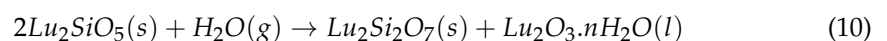
as a two-layer system with a silicon bond coat and pore-free ytterbium disilicate (YbDS; $\text{Yb}_2\text{Si}_2\text{O}_7$) as topcoat. This two-layer system was deposited on an a-SiC substrate using an optimized air plasma spray approach. The coating system was well matched to the substrate in terms of coefficients of thermal expansion (CTE), furthermore YbDS shows a moderate resistance to form silicon hydroxide vapour in water vapour-rich environments. The test results showed that slow steam volatilization of the YbDS topcoat resulted in the formation of a thin, partially protective, high CTE YbMS outside the YbDS. Progressive edge degradation of EBCs was observed during the steam thermal cycling exposure period, which is consistent with water vapour volatilization of the TGO scale edges directly exposed to the environment.

Nasiri et al. [59] studied water vapour corrosion of rare earth monosilicates EBC exposed to 1350 °C for 50, 100 and 166 h in a tube furnace. It was observed that Y, Er, Yb and Lu-silicates show little weight change after 166 h exposure if compared to Gd-silicate. XRD analysis illustrated that the test oxides have a mix of both mono and disilicates after 50 h exposure to water vapour to form disilicate. It was found that Gd-silicate was completely converted $\text{Gd}_{4.67}\text{Si}_3\text{O}_{13}$ silicate after 5+0 h water vapour exposure, thus leading to unsuitable EBC for application. Microstructures of Er, Y, Yb and Lu-silicates after testing show characteristics of protruding ridges and cracks, while the Gd-silicate appears significantly melted and contains striped contrast grains suggestive of a Gd/Si homologous series.

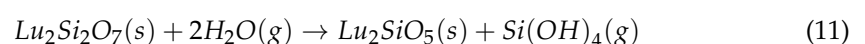
Eaton and Linsey [60] conducted the water vapour corrosion tests of yttrium silicates at 1200 °C in a 90 vol.% H_2O –10 vol.% O_2 condition but did not observe weight gain after 500 h exposure, while Lee et al. [45] observed a weight gain of $\sim 3\text{--}6 \times 10^{-3}$ mg/cm²h in Y_2SiO_5 , $\text{Y}_2\text{Si}_2\text{O}_7$ and Y_2O_3 samples exposed at 1500 °C under 50 vol.% H_2O –50 vol.% O_2 for 100 h. Liu et al. [61] studied the water vapour corrosion resistance at 1400 °C under 50 vol.% H_2O –50 vol.% O_2 for 400 h on bulk yttrium-silicate specimens containing Y_2SiO_5 and $\text{Y}_2\text{Si}_2\text{O}_7$ phases. It was suggested that yttrium monosilicate reacts with oxygen during water vapour to form disilicate, according to Equation (9),



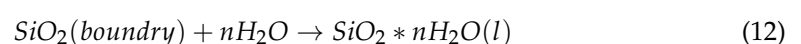
Ueno et al. [57] conducted similar observations on $\text{Lu}_2\text{Si}_2\text{O}_7$ bulk samples tested at 1500 °C for 100 h. They suggested that the decomposition of $\text{Lu}_2\text{Si}_2\text{O}_7$ to Lu_2SiO_5 was an early stage of the recession, subsequently followed by the reaction of Lu_2SiO_5 with water vapour to form $\text{Lu}_2\text{Si}_2\text{O}_7$ as Equation (10),



Ueno et al. [57] also tested the water vapour corrosion resistance for bulk $\text{Lu}_2\text{Si}_2\text{O}_7$ /mullite eutectic without grain boundary phases at 1300 °C for 100 h under 30 vol.% H_2O –70 vol.% O_2 . It was found that decomposition of $\text{Lu}_2\text{Si}_2\text{O}_7$ into Lu_2SiO_5 occurred only near the surfaces according to Equation (11):

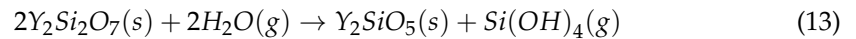


In another study, Ueno et al. [62] showed that the water vapour corrosion rate of $\text{Yb}_2\text{Si}_2\text{O}_7$ is higher than that of $\text{Lu}_2\text{Si}_2\text{O}_7$, in which the silica grain boundary glass was removed after water vapour corrosion at 1500 °C for 50 h under 30 vol.% H_2O –70 vol.% O_2 . It was demonstrated that the silica glass-rich melted areas were induced by decreasing the melting temperature of the boundary with increasing H_2O content [63]. Liquid SiO_2 was formed following Equation (12), which is in agreement with the results of Maier et al. [64],

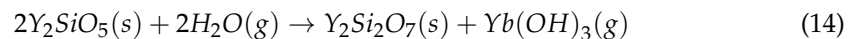


Ueno et al. [58] observed recession of $\text{Yb}_2\text{Si}_2\text{O}_7$ occurred between 1300 °C and 1500 °C after 500 h under 30 vol.% H_2O –70 vol.% O_2 , where $\text{Yb}_2\text{Si}_2\text{O}_7$ decomposed into Yb_2SiO_5

following Equation (13). $\text{Yb}_2\text{Si}_2\text{O}_7$ samples formed the porous structure due to the decomposition of $\text{Yb}_2\text{Si}_2\text{O}_7$ induced by water vapour attack of grain boundary glassy phase. Cracks occurred in samples and they corroded after 500 h at 1400 °C due to tensile stresses induced by the decomposition of $\text{Yb}_2\text{Si}_2\text{O}_7$,



Exposed for over 500 h at 1500 °C under 30 vol.% H_2O –70 vol.% O_2 , porous structures, however, no longer exist possibly due to the reaction of Equation (14) in which hydroxide formed,



Maier et al. [64] examined the water vapour corrosion behaviour of EBCs that contain both $\text{Yb}_2\text{Si}_2\text{O}_7$ and Yb_2SiO_5 exposed at 1500 °C for 310 h under a 30 vol.% H_2O –70 vol.% O_2 condition. The corroded samples were found with a coverage of rare earth aluminum garnet $\text{Yb}_2\text{Al}_5\text{O}_{12}$, and, meanwhile, showed the grain boundary attack of $\text{Yb}_2\text{Si}_2\text{O}_7$ in lutetium disilicate [64]. In addition, monosilicate was formed with an increase during the exposure period. However, this is a contradiction in the literature regarding the water vapour behavior of Er-silicates. For example, Ueno et al. [57] examined bulk samples containing both $\text{Er}_2\text{Si}_2\text{O}_7$ and Er_2SiO_5 under 30 vol.% H_2O –70 vol.% O_2 at 1500 °C for 100 h, and found the samples completely melted after the corrosion test. In another example, however, Lee et al. [45] did not observe significant weight gain on test samples that contain $\text{Er}_2\text{Si}_2\text{O}_7$, Er_2SiO_5 , and Er_2O_3 after 100 h exposure at 1500 °C under 50 vol.% H_2O and 50 vol.% O_2 water vapour condition.

Lu et al. [65] examined the formation and growth of silica scale beneath environmental barrier coatings tested under high temperature water-vapour environment, where the corroded EBCs coated C/SiC composites were observed under the water vapor attack, Figure 12. It was found that at high water-vapour partial pressures, the dominant oxidant for TGO scale growth was H_2O , and EBCs were observed to serve as a water-bearing layer to insulate water vapour attack from beneath the composites and also a barrier layer retarding the diffusion of oxidants to the EBC/bond coating.

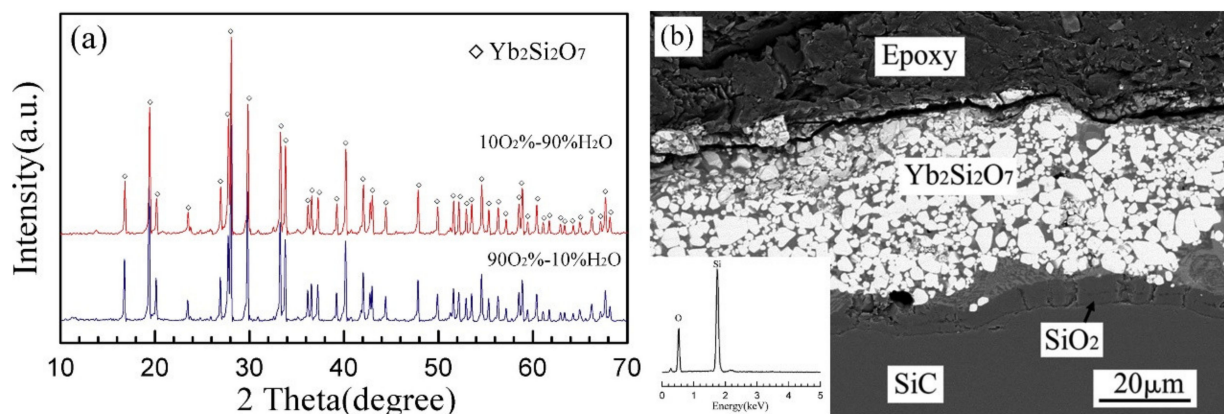


Figure 12. X-ray diffraction (XRD) patterns and typical SEM cross-section morphologies of $\text{Yb}_2\text{Si}_2\text{O}_7$ coated on C/SiC after water-vapor corrosion at 1250 °C under 90 vol.% O_2 –10 vol.% H_2O and 10 vol.% O_2 –90 vol.% H_2O : (a) XRD patterns after corrosion for 200 h, and (b) SEM cross-section after corrosion for 100 h under 10 vol.% O_2 –90 vol.% H_2O [65].

Golden et al. [50] examined the thermochemical stability of $\text{Y}_2\text{Si}_2\text{O}_7$ via a test in a high-temperature, high-velocity water vapour environment to better understand the mechanisms of SiO_2 scale depletion. The spark plasma sintered $\text{Y}_2\text{Si}_2\text{O}_7$ specimens were fabricated and then exposed in a steam-jet furnace at 1000 °C and 1200 °C for 3–250 h and steam velocities of 131–174 m/s under 1 atm H_2O pressure. The test results showed

a selective volatilization of SiO_2 scale to form volatile $\text{Si}(\text{OH})_4$ (g) and porous Y_2SiO_5 . Diffusion of H_2O (g) and $\text{Si}(\text{OH})_4$ (g) through pores by molecular diffusion mode and Knudsen diffusion was identified.

Sun et al. [66] evaluated high-temperature corrosion of $(\text{Er}_{0.25}\text{Tm}_{0.25}\text{Yb}_{0.25}\text{Lu}_{0.25})_2\text{Si}_2\text{O}_7$ environmental barrier coatings subjected to water vapor attack, where the tests were conducted at 1400°C for 4 h. The results demonstrated that the $(4\text{RE}_{0.25})_2\text{Si}_2\text{O}_7$ disilicate shows a superior water vapour corrosion resistance compared with those of $\text{Ba}_{0.5}\text{Sr}_{0.5}\text{Al}_2\text{Si}_2\text{O}_8$ and $\text{Ba}_{0.75}\text{Sr}_{0.25}\text{Al}_2\text{Si}_2\text{O}_8$. A correlation between the water contact angles and the high-temperature water vapour resistance was established and referred to as a reasonable guideline for the preliminary selection or screening of RE disilicates for hot water resistance capability. It may be concluded that the multicomponent RE disilicate shows better water vapor corrosion resistance and possess promising EBC applications.

Wang et al. [67] studied water vapour corrosion behavior of Yb_2SiO_5 environmental barrier coatings fabricated by plasma spray-physical vapour deposition (PS-PVD). Figure 13 illustrates schematically the structural evolution of Yb_2SiO_5 coating due to water vapour corrosion. The corrosion failure behaviour of the coating system in the steam environment after heat treatment at 1300°C was examined, in which good temperature stability and water vapour corrosion resistance were observed for ytterbium silicate. The topcoat decomposition of ytterbium silicate was found to damage the coatings, and at 1300°C , the water vapour reacts with the decomposed inclusions in the coating and continuously penetrates the substrate leading to the formation of a porous network structure. Such a porous network structure makes the coating brittle and results in microscopic cracks. Hence, this suggested that the compact environmental barrier coatings can be prepared by plasma spray-physical vapour deposition.

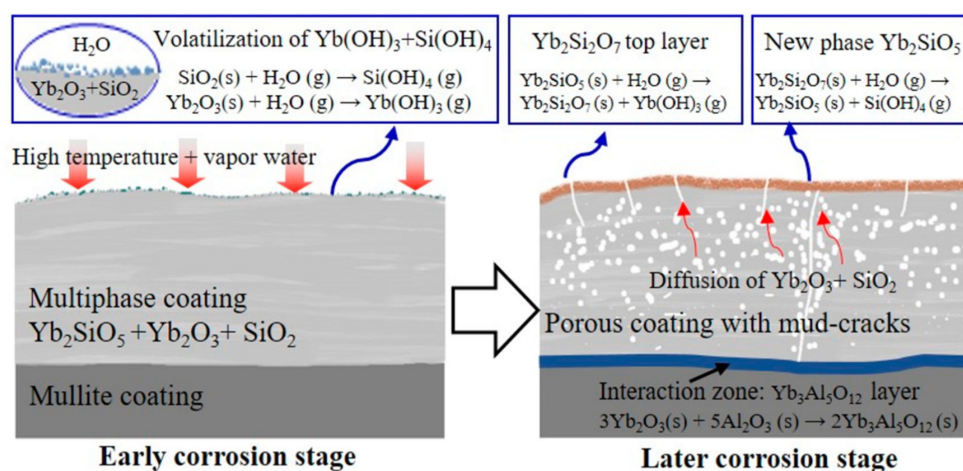


Figure 13. Structural evolution model of vapor corrosion of Yb_2SiO_5 coating [67].

Yang et al. [68] examined the thermal shock resistance and bonding strength of tri-layer Yb_2SiO_5 /mullite/Si coating on SiCf/SiC composites under thermal cycling test (TCT) (from a high temperature of 1200°C to a low temperature of 200°C in water vapour with 50 vol.% H_2O and 50 vol.% O_2). After 685 cycles of test, the weight loss of the coating system was found to be $\sim 0.1\%$. The significant weight loss was observed after 700 cycles of TCT due to coating exfoliation rather than due to $\text{Si}(\text{OH})_4$ steam generation. The bonding strength between tri-layers coating and SiCf/SiC substrate was also observed to gradually decrease as more TCT was performed. After 700 TCT, the bonding strength was reduced from the initial 12.28 MPa to the 6.79 MPa, due to the formation of vertical and horizontal cracks between the coating and the substrate. The damage generated during TCT determines the rupture of bonding between coating and substrate. As more TCT was conducted, the failure mode of tri-layers coating during TCT tensile test was gradually changed from the

dominant debonding between Si and SiCf/SiC to the dominant debonding between Si and outer layers due to the generation of horizontal cracks between Si layers and outer layers.

Ruggles-Wrenn et al. [69] studied the fatigue behaviour of the ytterbium disilicate environmental barrier coating on a SiC/SiC ceramic composite at elevated temperatures. The tension-tension fatigue property of the EBC-containing composite was examined in both air and steam at 1200 °C. It was observed that in the air, the EBC system shows a lower fatigue limit and a shorter cyclic life than the uncoated CMC. The reduced fatigue performance in the air of the EBC containing composite was due to its reduced tensile strength. The EBC/Hi-N/MI-SiC system, however, suffers no degradation of fatigue performance due to steam. It was also found that the fatigue with runout of 200,000 cycles was achieved at 110 MPa (~50%UTS) in both air and steam, and cyclic lives produced in steam are similar to those produced in the air. Previous cyclic loadings cause a minimal degradation of tensile strength of the EBC-containing composite with minor damage to the fibers. The $\text{Yb}_2\text{Si}_2\text{O}_7$ coating was found to successfully protect the CMC composite against the environmental attack at 1200 °C in both air and steam. The oxidation-induced cracks do not cause damage and failure of the EBC system, instead, the cracks initiate from numerous voids in the interior of the EBC/Hi-N/MI-SiC composite.

Kowalski et al. [70] studied thermally grown oxide in water vapour environment on both coated and uncoated SiC. Specifically, the test coupons of SiC and SiO_2 were thermally cycled in a flowing steam of 90 vol.%/10 vol.% $\text{H}_2\text{O}/\text{O}_2$ at 1426 °C aiming to simulate a turbine environment's water vapour partial pressure. The established parilinear model for oxidation and volatilization was examined and used to describe the oxidation process. A condensed version of the model was proposed to extract both the oxidation kinetic rate constant (k_p) and volatilization rate constant (k_1) by using a few measured data in a short period window. Because of a high $\text{Si}(\text{OH})_4$ (g) volatility rate, the SiO_2 scale thickness approached nearly invariant parilinear limiting values (~3–6 μm) for all test conditions. However, there still existed a disparity between the weight changes measured and the thickness of the resulting oxide scale, and the contribution from the material properties to the oxidation and volatilization rates.

4.4. Recession Evaluation on EBC Topcoat and TGO Scale

By carrying out first-principles total energy calculations, Han et al. [71] studied the water vapour corrosion resistance of selected rare earth monosilicates RE_2SiO_5 (RE: Lu, Yb, Tm, Er, Ho, Dy, Y and Sc) [71–73]. By evaluating the Mulliken population values of Si–O bonds, it seems that the rare earth monosilicates show a similar water vapour corrosion resistance, with an exception of Lu_2SiO_5 that illustrates much lower water vapour corrosion resistance. A strategy was then proposed to improve the water vapour corrosion resistance of RE_2SiO_5 by doping the second rare earth elements on the RE sites. Following this strategy, a number of calculations were conducted with the first one of using different rare earth element dopants, i.e., Lu, Er, Y, and Sc, to substitute a half mole proportion of Yb in the Yb_2SiO_5 lattice; while the second one of using Sc as a dopant to substitute a half mole proportion of rare earth elements in different rare earth monosilicates, i.e., Lu_2SiO_5 , Er_2SiO_5 and Y_2SiO_5 . It was found that the Sc substitution of Yb_2SiO_5 can greatly improve its water vapor resistance, whereas the substitution of Lu, Er and Y for Yb in Yb_2SiO_5 achieve a limited effect. Moreover, the Sc substitution for Y in Y_2SiO_5 can noticeably improve its water vapor corrosion resistance, and it is interesting to note that the solid solution of ScYSiO_5 behaves with the best water vapor resistance in these selected rare earth monosilicates. These results assess the water vapor resistance of the rare earth monosilicates and demonstrate that doping on the RE site could possibly further improve its water vapor resistance, in which the results could provide useful information for the selection of environmental barrier coating topcoat materials with better water vapor corrosion resistance.

Smialek et al. [74] investigated the recession of SiC and Si_3N_4 resulting from the SiO_2 scale volatility in combustion environments, where SiC and Si_3N_4 were tested under

selected turbine engine combustion conditions, with an intention to reflect either conventional fuel-lean or fuel-rich mixtures for high-speed aircraft. For all the test cases, protective SiO₂ scales were found to form, and the parabolic growth kinetics, i.e., parabolic growth moderated simultaneously by the linear volatilization, was found to describe the volatility of the SiO₂ scale well. It was observed that the recession rates produced by furnace tests agreed with the model evaluated based on Si(OH)₄ (fuel-lean) or SiO (fuel-rich) volatile species. The rates produced by the high-pressure burner rig (HPBR) pressure and velocity dependencies also suggested volatilization phenomena. Better regression functional forms can be obtained to fit the recession rates: the recession is higher under fuel-rich HPBR than that under fuel-lean conditions; and both processes will lead to significant recession after long-term exposures. It was also found that the critical fuel-lean species is Si(OH)₄ under furnace and burner rig conditions but is known to be SiO only for the fuel-rich furnace (atmospheric) condition.

5. Conclusions

As demonstrated in the proceeding sections, the variability in costs of jet fuels, the need to secure fuel supplies, and the potential environmental benefits have demonstrated the need for investigations of sustainable alternative fuels for aviation. Understanding the critical impact of alternative fuels on hot section components will provide for gas turbine industry with strategic options in sustainability and maintainability of the existing and new fleets. The alternative fuels with a high ratio of hydrogen/carbon can produce more water vapour than the conventional jet fuels upon combustion. Although this provides benefits in terms of reduced particulate emissions, increased water vapour level of the fuels can exert a significant impact on hot section components. With alternative jet fuels used for aero-engines, the major impact on hot section components of gas turbines is severe hot corrosion via a reaction of water vapor with protective oxide scales. In the case of oxidation-resistant overlayer coatings of MCrAlY, more transient oxides are formed, leading to more and thicker spinel formation and thus reducing the development of continuous protective alumina scales (α -Al₂O₃). These spinels can adversely weaken the adherence of protective α -Al₂O₃ scales to the alloy substrate, causing the interfacial toughness of α -Al₂O₃/alloy to be decreased.

High-temperature water vapor has a significant effect on EBC performance and durability. It reduces the EBCs life via oxidation and recession processes during service. Rapid volatilization of SiC under combustion environments occurs through the reaction with water vapour at high temperature to form gaseous silicon hydroxides. Subsequently, this also affect each layer in the EBC, leading to cracking or delamination during thermal cycles. Ytterbium silicate-based oxides show good temperature stability and water vapour corrosion resistance. New types of EBC are needed to substantially enhance the life of hot section components of gas turbine engines.

Author Contributions: K.C.: Conceptualization, Methodology, Writing—original draft, Project administration, Resources, Funding acquisition. D.S.: Writing—review and editing. P.C.: Conceptualization, Writing—review and editing, Project administration, Resources, Funding acquisition. All authors have read and agreed to the published version of the manuscript.

Funding: This research is financially supported by DND DTAES through the DTS-SCS of National Research Council Canada via A1-014745 project.

Institutional Review Board Statement: Not applicable.

Informed Consent Statement: Not applicable.

Data Availability Statement: Data will be made available on reasonable request.

Conflicts of Interest: The authors report no declarations of interest.

References

1. Lefebvre, A.H.; Ballal, D.R. *Gas Turbine Combustion*; CRC Press/Taylor Francis: Boca Raton, FL, USA, 2010.
2. Braun-Unkhoff, M.; Riedel, U. Alternative fuels in aviation. *CEAS Aeronaut. J.* **2015**, *6*, 83–93. [[CrossRef](#)]
3. Kurzawska, P.; Jasiński, R. Overview of sustainable aviation fuels with emission characteristic and particles emission of the turbine engine fueled ATJ blends with different percentages of ATJ fuel. *Energies* **2021**, *14*, 1858. [[CrossRef](#)]
4. Maris-Sida, M.C.; Meier, G.H.; Pettit, F.S. Some water vapor effects during the oxidation of alloys that are α -Al₂O₃ formers. *Metall. Mater. Trans. A Phys. Metall. Mater. Sci.* **2003**, *34*, 2609–2619. [[CrossRef](#)]
5. Saunders, S.R.J.; Monteiro, M.; Rizzo, F. The oxidation behaviour of metals and alloys at high temperatures in atmospheres containing water vapour: A review. *Prog. Mater. Sci.* **2008**, *53*, 775–837. [[CrossRef](#)]
6. Sullivan, M.H.; Mumm, D.R. Vapor-Phase-Mediated Phenomena Associated with High Temperature, High Water Content Oxidation of MCrAlX Bond Coats. *Oxid. Met.* **2014**, *82*, 1–20. [[CrossRef](#)]
7. Sullivan, M.H.; Mumm, D.R. Transient stage oxidation of MCrAlY bond coat alloys in high temperature, high water vapor content environments. *Surf. Coat. Technol.* **2014**, *258*, 963–972. [[CrossRef](#)]
8. Giggins, C.S.; Pettit, F.S. Oxidation of Ni-Cr-Al Alloys Between 1000° and 1200 °C. *J. Electrochem. Soc.* **1971**, *118*, 1782. [[CrossRef](#)]
9. Wallwork, G.R.; Hed, A.Z. Some limiting factors in the use of alloys at high temperatures. *Oxid. Met.* **1971**, *3*, 171–184. [[CrossRef](#)]
10. Nijdam, T.J.; Kwakernaak, C.; Sloof, W.G. The effects of alloy microstructure refinement on the short-term thermal oxidation of NiCoCrAlY alloys. *Metall. Mater. Trans. A Phys. Metall. Mater. Sci.* **2006**, *37*, 683–693. [[CrossRef](#)]
11. Choi, H.; Yoon, B.; Kim, H.; Lee, C. Isothermal oxidation of air plasma spray NiCrAlY bond coatings. *Surf. Coat. Technol.* **2002**, *150*, 297–308. [[CrossRef](#)]
12. Shillington, E.A.; Clarke, D. Spalling failure of a thermal barrier coating associated with aluminum depletion in the bond-coat. *Acta Mater.* **1999**, *47*, 1297–1305. [[CrossRef](#)]
13. Angle, J.P.; Morgan, P.E.D.; Mecartney, M.L. Water vapor-enhanced diffusion in alumina. *J. Am. Ceram. Soc.* **2013**, *96*, 3372–3374. [[CrossRef](#)]
14. Zhou, C.; Yu, J.; Gong, S.; Xu, H. Influence of water vapor on the isothermal oxidation behavior of low pressure plasma sprayed NiCrAlY coating at high temperature. *Surf. Coat. Technol.* **2002**, *161*, 86–91. [[CrossRef](#)]
15. Kaplin, C.; Brochu, M. Effects of water vapor on high temperature oxidation of cryomilled NiCoCrAlY coatings in air and low-SO₂ environments. *Surf. Coat. Technol.* **2011**, *205*, 4221–4227. [[CrossRef](#)]
16. Stolle, R. Conventional and advanced coatings for turbine airfoils. *MTU Aero Engines* **2010**.
17. Haynes, J.A.; Unocic, K.A.; Pint, B.A. Effect of water vapor on the 1100 °C oxidation behavior of plasma-sprayed TBCs with HVOF NiCoCrAlX bond coatings. *Surf. Coat. Technol.* **2013**, *215*, 39–45. [[CrossRef](#)]
18. Rudolph, M.; Renusch, D.; Zschau, H.E.; Schütze, M. The effect of moisture on the delayed spallation of thermal barrier coatings: VPS NiCoCrAlY bond coat + APS YSZ top coat. *Mater. High Temp.* **2009**, *26*, 325–329. [[CrossRef](#)]
19. Déneux, V.; Cadoret, Y.; Hervier, S.; Monceau, D. Effect of Water Vapor on the Spallation of Thermal Barrier Coating Systems During Laboratory Cyclic Oxidation Testing. *Oxid. Met.* **2010**, *73*, 83–93. [[CrossRef](#)]
20. Smialek, J.L. Moisture-induced delayed spallation and interfacial hydrogen embrittlement of alumina scales. *Jom* **2006**, *58*, 29–35. [[CrossRef](#)]
21. Pint, B.A.; Garner, G.W.; Lowe, T.M.; Haynes, J.A.; Zhang, Y. Effect of increased water vapor levels on TBC lifetime with Pt-containing bond coatings. *Surf. Coat. Technol.* **2011**, *206*, 1566–1570. [[CrossRef](#)]
22. Zhou, C.; Yu, J.; Gong, S.; Xu, H. Influence of water vapor on the high temperature oxidation behavior of thermal barrier coatings. *Mater. Sci. Eng. A* **2003**, *348*, 327–332. [[CrossRef](#)]
23. Haynes, J.A.; Unocic, K.A.; Lance, M.J.; Pint, B.A. Impact of superalloy composition, bond coat roughness and water vapor on TBC lifetime with HVOF NiCoCrAlYHfSi bond coatings. *Surf. Coat. Technol.* **2013**, *237*, 65–70. [[CrossRef](#)]
24. Yanar, N.M.; Stiger, M.J.; Maris-Sida, M.; Pettit, F.S.; Meier, G.H. Effects of high temperature exposure on the durability of thermal barrier coatings. *Key Eng. Mater.* **2001**, *197*, 145–163. [[CrossRef](#)]
25. Chen, W.R.; Wu, X.; Marple, B.R.; Patnaik, P.C. Oxidation and crack nucleation/growth in an air-plasma-sprayed thermal barrier coating with NiCrAlY bond coat. *Surf. Coat. Technol.* **2005**, *197*, 109–115. [[CrossRef](#)]
26. Goward, G. Progress in coatings for gas turbine airfoils. *Surf. Coat. Technol.* **1998**, *108–109*, 73–79. [[CrossRef](#)]
27. Salazar, A.; Gómez-García, J.; Poza, P.; Utrilla, V. Microstructural Evolution of Thermal Barrier Coatings during Isothermal Oxidation. *Key Eng. Mater.* **2007**, *333*, 269–272. [[CrossRef](#)]
28. Tamura, M.; Takahashi, M.; Ishii, J.; Suzuki, K.; Sato, M.; Shimomura, K. Multilayered thermal barrier coating for land-based gas turbines. *J. Therm. Spray Technol.* **1999**, *8*, 68–72. [[CrossRef](#)]
29. Bennett, A. Properties of thermal barrier coatings. *Mater. Sci. Technol.* **1986**, *2*, 257–261. [[CrossRef](#)]
30. Lance, M.J.; Unocic, K.A.; Haynes, J.A.; Pint, B.A. Effect of water vapor on thermally-grown alumina scales on Pt-modified and simple aluminide bond coatings. *Surf. Coat. Technol.* **2013**, *237*, 2–7. [[CrossRef](#)]
31. Fontana, S.; Chevalier, S.; Caboche, G. Metallic interconnects for solid oxide fuel cell: Effect of water vapour on oxidation resistance of differently coated alloys. *J. Power Sources* **2009**, *193*, 136–145. [[CrossRef](#)]
32. Reed, R.C. *The Superalloys: Fundamentals and Applications*; Cambridge University Press: Cambridge, UK, 2006.
33. Unocic, K.A.; Pint, B.A. Effect of water vapor on thermally grown alumina scales on bond coatings. *Surf. Coat. Technol.* **2013**, *215*, 30–38. [[CrossRef](#)]

34. Gleeson, B. Thermal barrier coatings for aeroengine applications. *J. Propuls. Power* **2006**, *22*, 375–383. [[CrossRef](#)]
35. Pint, B.A.; Unocic, K.A.; Haynes, J.A. The effect of environment on TBC lifetime. In *Ceramics, controls, diagnostics and instrumentation, education, manufacturing materials and metallurgy, honors and awards, Proceedings of ASME Turbo Expo 2015, Montreal, Quebec, Canada, 15–19 June 2015*; GT2015-43762; ASME: New York, NY, USA, 2015; pp. 1–10. [[CrossRef](#)]
36. Pint, B.A.; Haynes, J.A. Effect of water vapour content on thermal barrier coating lifetime. *Mater. Sci. Technol.* **2013**, *29*, 828–834. [[CrossRef](#)]
37. Eriksson, R.; Yuan, K.; Li, X.H.; Lin Peng, R. Corrosion of NiCoCrAlY Coatings and TBC Systems Subjected to Water Vapor and Sodium Sulfate. *J. Therm. Spray Technol.* **2015**, *24*, 953–964. [[CrossRef](#)]
38. Wu, Y.; Narita, T. The cyclic oxidation behavior of the single crystal TMS-82+ superalloy in humidified air. *Mater. Corros.* **2009**, *60*, 781–787. [[CrossRef](#)]
39. Song, P.; He, X.; Xiong, X.; Ma, H.; Song, Q.; Lü, J.; Lu, J. Effect of water vapor on evolution of a thick Pt-layer modified oxide on the NiCoCrAl alloy at high temperature. *Mater. Res. Express* **2018**, *5*, 036514. [[CrossRef](#)]
40. Zhou, C.; Xu, H.; Gong, S. Influence of water vapor on the cyclic-oxidation behavior of a low-pressure plasma-sprayed NiCrAlY coating. *Oxid. Met.* **2004**, *62*, 195–206. [[CrossRef](#)]
41. Duan, W.; Song, P.; Li, C.; Huang, T.; Ge, Z.; Feng, J.; Lu, J. Effect of water vapor on the failure behavior of thermal barrier coating with Hf-doped NiCoCrAlY bond coating. *J. Mater. Res.* **2019**, *34*, 2653–2663. [[CrossRef](#)]
42. Clarke, D.R.; Oechsner, M.; Padture, N.P. Thermal-barrier coatings for more efficient gas-turbine engines. *MRS Bull.* **2012**, *37*, 891–898. [[CrossRef](#)]
43. Padture, N.P. Advanced structural ceramics in aerospace propulsion. *Nat. Mater.* **2016**, *15*, 804–809. [[CrossRef](#)] [[PubMed](#)]
44. Langston, L.S. Anticipated but Unwelcome. *Mech. Eng.* **2018**, *140*, 37–41. [[CrossRef](#)]
45. Lee, K.N.; Fox, D.S.; Bansal, N.P. Rare earth silicate environmental barrier coatings for SiC/SiC composites and Si₃N₄ ceramics. *J. Eur. Ceram. Soc.* **2005**, *25*, 1705–1715. [[CrossRef](#)]
46. Ohji, T.; Singh, M. (Eds.) *Engineered Ceramics*; John Wiley & Sons, Inc.: Hoboken, NJ, USA, 2016.
47. Jacobson, N.S. Corrosion of Silicon-Based Ceramics in Combustion Environments. *J. Am. Ceram. Soc.* **1993**, *76*, 3–28. [[CrossRef](#)]
48. Opila, E.J.; Hann, R.E. Paralineer oxidation of CVD SiC in water vapor. *J. Am. Ceram. Soc.* **1997**, *80*, 197–205. [[CrossRef](#)]
49. Richards, B.T.; Young, K.A.; De Francqueville, F.; Sehr, S.; Begley, M.R.; Wadley, H.N.G. Response of ytterbium disilicate-silicon environmental barrier coatings to thermal cycling in water vapor. *Acta Mater.* **2016**, *106*, 1–14. [[CrossRef](#)]
50. Golden, R.A.; Mueller, K.; Opila, E.J. Thermochemical stability of Y₂Si₂O₇ in high-temperature water vapor. *J. Am. Ceram. Soc.* **2020**, *103*, 4517–4535. [[CrossRef](#)]
51. Zhu, D.; Lee, K.N.; Miller, R.A. Cyclic Failure Mechanisms of Thermal and Environmental Barrier Coating Systems under Thermal Gradient Test Conditions. In *26th Annual International Conference on Advanced Ceramics and Composite*; NASA/TM: Cleveland, OH, USA, 2002.
52. Garcia, E.; Sotelo-Mazon, O.; Poblano-Salas, C.A.; Trapaga, G.; Sampath, S. Characterization of Yb₂Si₂O₇–Yb₂SiO₅ composite environmental barrier coatings resultant from in situ plasma spray processing. *Ceram. Int.* **2020**, *46*, 21328–21335. [[CrossRef](#)]
53. Lv, B.; Qu, Z.; Xu, B.; Wang, Y.; Fang, D. Water vapor volatilization and oxidation induced surface cracking of environmental barrier coating systems: A numerical approach. *Ceram. Int.* **2021**, *47*, 16547–16554. [[CrossRef](#)]
54. Robinson, R.C.; Smialek, J.L. SiC recession caused by SiO₂ scale volatility under combustion conditions: I. Experimental results and empirical model. *J. Am. Ceram. Soc.* **1999**, *82*, 1817–1825. [[CrossRef](#)]
55. Opila, E.J. Oxidation and volatilization of silica formers in water vapor. *J. Am. Ceram. Soc.* **2003**, *86*, 1238–1248. [[CrossRef](#)]
56. Lee, K.N. Key Durability Issues With Mullite-Based Environmental Barrier Coatings for Si-Based Ceramics. *J. Eng. Gas Turbines Power* **2000**, *122*, 632–636. [[CrossRef](#)]
57. Ueno, S.; Jayaseelan, D.D.; Ohji, T. Development of oxide-based EBC for silicon nitride. *Int. J. Appl. Ceram. Technol.* **2004**, *1*, 362–373. [[CrossRef](#)]
58. Ueno, S.; Ohji, T.; Lin, H.T. Recession behavior of Yb₂Si₂O₇ phase under high speed steam jet at high temperatures. *Corros. Sci.* **2008**, *50*, 178–182. [[CrossRef](#)]
59. Al Nasiri, N.; Patra, N.; Jayaseelan, D.D.; Lee, W.E. Water vapour corrosion of rare earth monosilicates for environmental barrier coating application. *Ceram. Int.* **2017**, *43*, 7393–7400. [[CrossRef](#)]
60. Eaton, H.E.; Linsey, G.D. Accelerated oxidation of SiC CMC's by water vapor and protection via environmental barrier coating approach. *J. Eur. Ceram. Soc.* **2002**, *22*, 2741–2747. [[CrossRef](#)]
61. Liu, J.; Zhang, L.; Hu, F.; Yang, J.; Cheng, L.; Wang, Y. Polymer-derived yttrium silicate coatings on 2D C/SiC composites. *J. Eur. Ceram. Soc.* **2013**, *33*, 433–439. [[CrossRef](#)]
62. Ueno, S.; Jayaseelan, D.D.; Ohji, T. Comparison of water vapor corrosion behavior of silicon nitride with various EBC layers. *J. Ceram. Process. Res.* **2004**, *5*, 355–359.
63. Kennedy, G.C.; Wasserburg, G.J.; Heard, H.C.; Newton, R.C. The upper three-phase region in the system SiO₂–H₂O. *Am. J. Sci.* **1962**, *260*, 501–521. [[CrossRef](#)]
64. Maier, N.; Nickel, K.G.; Rixecker, G. High temperature water vapour corrosion of rare earth disilicates (Y,Yb,Lu)₂Si₂O₇ in the presence of Al(OH)₃ impurities. *J. Eur. Ceram. Soc.* **2007**, *27*, 2705–2713. [[CrossRef](#)]
65. Lu, Y.; Wang, Y. Formation and growth of silica layer beneath environmental barrier coatings under water-vapor environment. *J. Alloys Compd.* **2018**, *739*, 817–826. [[CrossRef](#)]

66. Wang, C.; Liu, M.; Feng, J.; Zhang, X.; Deng, C.; Zhou, K.; Zeng, D.; Guo, S.; Zhao, R.; Li, S. Water vapor corrosion behavior of Yb_2SiO_5 environmental barrier coatings prepared by plasma spray-physical vapor deposition. *Coatings* **2020**, *10*, 392. [[CrossRef](#)]
67. Sun, L.; Luo, Y.; Tian, Z.; Du, T.; Ren, X.; Li, J.; Hu, W.; Zhang, J.; Wang, J. High temperature corrosion of $(\text{Er}_{0.25}\text{Tm}_{0.25}\text{Yb}_{0.25}\text{Lu}_{0.25})_2\text{Si}_2\text{O}_7$ environmental barrier coating material subjected to water vapor and molten calcium–magnesium–aluminosilicate (CMAS). *Corros. Sci.* **2020**, *175*, 108881. [[CrossRef](#)]
68. Yang, H.; Yang, Y.; Cao, X.; Huang, X.; Li, Y. Thermal shock resistance and bonding strength of tri-layer Yb_2SiO_5 /mullite/Si coating on SiCf/SiC composites. *Ceram. Int.* **2020**, *46*, 27292–27298. [[CrossRef](#)]
69. Ruggles-Wrenn, M.B.; Williams, T.M. Fatigue of a SiC/SiC ceramic composite with an ytterbium-disilicate environmental barrier coating at elevated temperature. *Int. J. Appl. Ceram. Technol.* **2020**, *17*, 2074–2082. [[CrossRef](#)]
70. Kowalski, B.; Harder, B. Thermally grown oxide in water vapor on coated and uncoated SiC. *J. Am. Ceram. Soc.* **2020**, *103*, 5978–5989. [[CrossRef](#)]
71. Han, J.; Wang, Y.; Liu, R.; Jiang, D. Study on water vapor corrosion resistance of rare earth monosilicates RE_2SiO_5 (RE = Lu, Yb, Tm, Er, Ho, Dy, Y, and Sc) from first-principles calculations. *Heliyon* **2018**, *4*, e00857. [[CrossRef](#)]
72. Wang, Y.; Liu, J. First-principles investigation on the corrosion resistance of rare earth disilicates in water vapor. *J. Eur. Ceram. Soc.* **2009**, *29*, 2163–2167. [[CrossRef](#)]
73. Wang, Y.; Liu, J. Corrosion of barium aluminosilicates by water-vapour: An investigation from first principles. *Corros. Sci.* **2009**, *51*, 2126–2129. [[CrossRef](#)]
74. Smialek, J.L.; Robinson, R.C.; Opila, E.J.; Fox, D.S.; Jacobson, N.S. SiC and Si_3N_4 recession due to SiO_2 scale volatility under combustor conditions. *Adv. Compos. Mater.* **1999**, *8*, 33–45. [[CrossRef](#)]